A more complete analysis would consider that the gas constant and the specific heat ratio of exhaust gases flowing in the turbine also vary. The gas constant of exhaust gases are estimated to be actually higher than the gas constant of air: 0.74% for natural gas burning and only 0.16% higher for biogas exhaust gases. Given this small variation, it can be assumed that effects on compressor matching due to gas constant variation of exhaust gases are negligible. The specific heat ratio cannot be considered the same as the specific heat ratio of air (1.345), since it results 1.311 for NG exhaust gases and 1.308 for biogas exhaust gases, the proper value must be used in either case.

3.2 Approximation

After the previous considerations, since the actual performance curves of compressor, turbine and regenerator may interplay differently, one can assume for an initial design phase that the compressor-turbine matching remains unaltered, as do the boundary conditions if fuel is changed. The only variations in boudary conditions to be considered being the fuel flow rate and its composition.

Chapter 4

Theoretical premixed combustion effects due to fuel change

This chapter describes how the two main properties of premixed flames, laminar flame speed and flame thickness, can be obtained based on a theoretical framework.

Understanding laminar flames is a necessary prerequisite to the study of turbulent flames, condition that dominates the flow field in the combustor we are designing. In both laminar and turbulent flows, the same physical processes are active, and many turbulent flame theories are based on an underlying laminar flame structure [53].

In a posterior moment, we will indicate how these properties correlate to useful parameters such as quenching distance, ignition energy and blowout and flashback tendencies since they aid in the design decisions regarding the injector.

The theoretical phenomena and equations described in this chapter will be solved numerically using Ansys Fluent software with proper solution schemes which are better described in chapter 7.

4.1 Governing equations for chemically reacting viscous flows

The fundamental physical principles that apply to any flow field, reactive or not are three:

- Mass is conserved;
- Newton's second law;
- Energy is conserved;

These physical principles are translated into the mathematical governing equations of the fluid dynamics. The mass conservation principle is represented by the *Continuity equation* (which in reactive flows is split into a finite number of *Species Conservation equations*); the Newton's second law is represented by the *Momentum equations* in the three spatial dimensions x, y, z for example, and the Energy conservation principle, also known as First Law of Thermodynamics is represented by the *Energy equation* (which in reactive flows needs to be expressed in terms of the *absolute enthapy* summed for all species involved in the reaction mechanism and needs to account for diffusive transport of the absolute enthalpy).

We'll present such partial differential equations in the conservation forms[1]. Note that the following equations relate to viscous flows, that's because molecular diffusion of species into the mixture, a phenomenon that occurs in the chemically reacting flows is inherently dissipative; i.e., it increases the entropy of the flow stream[2].

4.1.1 Continuity equation

In any flow field (reactive or non-reactive), the unsteady, compressible, three dimensional continuity equation expressed in conservation form with partial differentials is

$$\frac{\partial \rho}{\partial t} + \nabla(\rho \mathbf{V}) = 0 \tag{4.1}$$

Where we introduce four dependent variables, namely the specific mass of the mixture 'ρ' and the velocity '$\mathbf{V}$' which is composed by the three velocity components, in the Cartesian system we have $\mathbf{V} = u\mathbf{i} + v\mathbf{j} + w\mathbf{k}$. Equation (4.1) is also known as Global Continuity Equation.

Species conservation

In a reactive flow, the fluid particle is a mixture composed by various reactants and products. The number of species in the mixture is N while each species is denoted by a subscript i.

[1] Any equation derived based on a fixed finite or infinitesimal control volume, i.e. in the Euler framework, is considered by Computational Fluid Dynamicists as equations in the conservation form because they deal with fluxes instead of the independent variables directly and this approach is sometimes needed to find numerical solution for singularities that naturally arise in the flow field, the sudden increase of specific mass across a shock wave is an example; the non-conservation equations don't capture these conditions adequately.

[2] A viscous flow is one where the transport phenomena of friction, thermal conduction and/or mass diffusion are included[16].

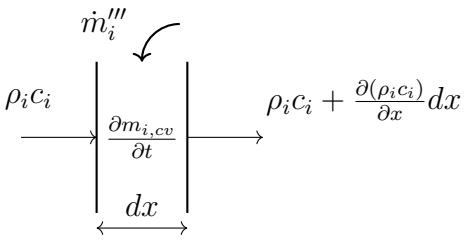

Figure 4.1: Species fluxes, generation and accumulation inside a simplified control volume with infinitesimal thickness dx.

The rate of increase of mass of species i within the control volume, $\frac{\partial m_{i,cv}}{\partial t}$, the mass flux of the species i in and out such control volume, and the species mass production rate $\dot{m}_i'''$ by chemical reaction (source term) inside the control volume are indicated in Figure 4.1. Here we consider for simplicity only flow in the x direction. The species velocity in this direction is denoted as 'c_i'

The net rate of increase in the mass of species i within the control volume relates to the mass fluxes and reaction rate as follows:

$$\frac{\partial m_{i,cv}}{\partial t} = \rho_i c_i dydz - \left(\rho_i c_i + \frac{\partial(\rho_i c_i)}{\partial x} dx\right) dydz + \dot{m}_i''' \cdot dxdydz \tag{4.2}$$

Equation (4.2) shows that the rate of increase of mass of species i within control volume must equal the net mass flow of species i into the control volume plus the mass production rate of species i by chemical reactions.

Observe that the term given by the chemical reaction rate $\dot{m}_i''' \cdot dxdydz$ is the source term. In addition, note that $\frac{\partial m_{i,cv}}{\partial t}$ is the local variation of mass of species i accounting for changes in the flow field with time. The remaining terms on the right are the advective net variation of mass of species i in the control volume that accounts for the movement of fluid from one region of the flow to another. Rearranging (4.2) to evidence the equation as a *transport equation*:

$$\dot{m}_i''' \cdot dxdydz = \frac{\partial m_{i,cv}}{\partial t} + \left[\left(\rho_i c_i + \frac{\partial(\rho_i c_i)}{\partial x} dx\right) - \rho_i c_i\right] dydz \tag{4.3}$$

We note that $m_{i,cv} = \rho Y_i dxdydz$, where Y_i represents the mass fraction of species i. Upon dividing by $dxdydz$, Equation (4.3) simplifies to:

$$\dot{m}_i''' = \frac{\partial \rho Y_i}{\partial t} + \frac{\partial(\rho_i c_i)}{\partial x} = \frac{\partial \rho_i}{\partial t} + \frac{\partial(\rho_i c_i)}{\partial x} \tag{4.4}$$

Because we are considering a reacting flow, the species velocity in the x-direction 'c_i' is given by the sum of average mixture velocity 'c' and the diffusion velocity of the species 'u_i' with respect to the mixture,

$$c_i = c + u_i \tag{4.5}$$

Where, by definition the average mixture velocity c is given by:

$$c = \Sigma Y_i c_i \tag{4.6}$$

The diffusive molecular flux $\rho_i u_i$ is given by Fick's Law:

$$\rho_i u_i = -\rho \mathcal{D}_{im} \frac{dY_i}{dx} \tag{4.7}$$

whose formula in a tri-dimensional space is

$$\rho_i \mathbf{U_i} = -\rho \mathcal{D}_{im} \nabla Y_i \tag{4.8}$$

where $\mathcal{D}_{im}$ is the mass diffusivity of species i and the mixture m pair, and $\mathbf{U_i}$ is the diffusion velocity vector of the species i. Upon considering that $\rho_i = \rho \cdot Y_i$, and by substituting Eqs. (4.5), (4.6) and (4.7) into Eq. (4.4) it's possible to express the species mass production rate as

$$\dot{m}_i''' = \frac{\partial \rho_i}{\partial t} + \frac{\partial}{\partial x}\left[\rho c Y_i - \rho \mathcal{D}_{im} \frac{dY_i}{dx}\right] \tag{4.9}$$

Where it's possible to identify inside the advective part, the convective (or bulk) flux term followed by the diffusive flux term.

Considering $\mathcal{D}_{im}$ a known parameter for all species, the added dependent variable in this subsection are 2 (two) for each species, namely, the species mass production rate by chemical reaction $\dot{m}_i'''$ and the species mass fraction Y_i. Thus, for a mixture with N species, the number of added dependent variables is $2N$.

Equation (4.4), for species production can be expressed in three dimensions as

$$\dot{m}_i''' = \frac{\partial \rho Y_i}{\partial t} + \nabla(\rho Y_i \mathbf{V} - \rho \mathcal{D}_{im} \nabla Y_i) \tag{4.10}$$

i.e.,

$$\dot{m}_i''' = \frac{\partial \rho_i}{\partial t} + \nabla(\rho_i \mathbf{V}_i) \tag{4.11}$$

Where $\rho_i \mathbf{V}_i = \dot{\mathbf{m}}_i''$ represents the flux of species i (including the convective and diffusive fluxes) in the three dimensions. Equation (4.10) is in conservation form

from the point of view of CFD and can be written for all the N species involved in the problem. Therefore, we still need to specify $2N - N = N$ equations to equalize the number of dependent variables added in the reactive flow.

Since the chemical reaction is known a priori, it's possible to obtain from the mass coefficients, $N - 1$ mass balance equations that relate the mass production of species[3]. To illustrate this and to proceed with the analysis of this chapter, we represent the global reaction indicated in the beginning of Chapter 6,

$$\mathrm{CH_4} + (\tfrac{\chi_{\mathrm{CO_2}}}{\chi_{\mathrm{CH_4}}})\mathrm{CO_2} + (\tfrac{\chi_{\mathrm{N_2}}}{\chi_{\mathrm{CH_4}}})\mathrm{N_2} + \tfrac{2}{\Phi}(\mathrm{O_2} + 3.76\,\mathrm{N_2}) \longrightarrow$$
$$(1 + \tfrac{\chi_{\mathrm{CO_2}}}{\chi_{\mathrm{CH_4}}})\mathrm{CO_2} + 2\,\mathrm{H_2O} + 2\,(\tfrac{1-\Phi}{\Phi})\mathrm{O_2} + (\tfrac{7.52}{\Phi} + \tfrac{\chi_{\mathrm{N_2}}}{\chi_{\mathrm{CH_4}}})\mathrm{N_2}.$$

as the simplified reaction

$$1\,\mathrm{F} + \nu\mathrm{Ox} \longrightarrow (\nu + 1)\,\mathrm{Pr}$$

Where the fuel 'F' is represented by $\mathrm{CH_4} + (\frac{\chi_{\mathrm{CO_2}}}{\chi_{\mathrm{CH_4}}})\mathrm{CO_2} + (\frac{\chi_{\mathrm{N_2}}}{\chi_{\mathrm{CH_4}}})\mathrm{N_2}$ (with the molar fractions obeying the relation $\chi_{\mathrm{CH_4}} + \chi_{\mathrm{CO_2}} + \chi_{\mathrm{N_2}} = 1$), the oxidant 'Ox' is represented by $\frac{2}{\Phi}(\mathrm{O_2} + 3.76\,\mathrm{N_2})$ and the products 'Pr' are represented by the right side of the reaction. The mass of oxidant to react with one kilogram of fuel is known and indicated by 'ν'.

Note that considering the simplified reaction the number of species is three. For which we can write two mass balance equations, all in terms of the mass species production (or consumption if it results negative) of the fuel:

$$\dot{m}'''_{Ox} = \nu \dot{m}'''_{F} \tag{4.12}$$

$$\dot{m}'''_{Pr} = -(\nu + 1)\dot{m}'''_{F} \tag{4.13}$$

The remaining equation to equalize the number of dependent variables added in the reactive flow comes from the *reaction rate* of the fuel species in this case. The reaction rate is known based on chemical kinetics of the global reaction[4]. The reaction rate of fuel species is expressed as

[3]If we are dealing with a reaction mechanism instead of a global reaction, it would be possible to write $N_j - 1$ equations for each reaction, where N_j represents the number of species present in the reaction j.

[4]If we are dealing with a reaction mechanism instead of a global reaction, the number of remaining equations is equal to the number of reactions and the remaining equations are the reaction rates of the species used to write the mass balances equations for each reaction.

$$\frac{D[F]}{Dt} = -k_G[F]^m[Ox]^n \tag{4.14}$$

Where $[F]$ represents the fuel molar concentration, k_G the rate coefficiet of the global reaction, m is the reaction order with respect to fuel and n is the reaction order with respect to the oxidant, both known a priori. Assuming that most combustion related elementary reactions are bimolecular, that as consequence, the global reaction has a similar behavior and if the temperature range of interest is not too large then the rate coefficient k_G can be expressed by the semi-empirical Arrhenius form $k_G = A \cdot exp[^{-E_a}/_{R_uT}]$, where T is the local temperature, A is the pre-exponential factor related to the reaction (known a priori; it can be evaluated as a function of local temperature), E_a is the reaction activation energy (known a priori), and $R_u = 8.31447kJ/kmol.K$ is the universal gas constant.

The conversion between the species mass production rate $\dot{m}'''_f$ and the mole production rate $\frac{D[F]}{Dt}$ is given by $\dot{m}'''_f = MW_f \frac{D[F]}{Dt}$. Where the molecular weight of fuel is known and the derivative of molar concentration is the substantial derivative[5].

Since the flow field dependent variable we have introduced is the mass fraction Y we present the conversion between the molar concentration and the mass fraction, by doing so the number of added variables equals the number of available equations and we can proceed with the other governing equations of the flow field. Taking our case as an example, where we explicit the fuel species, the molar concentration is related to the mass fraction by the relation

$$Y_F = \frac{[F]MW_F}{\rho} \tag{4.15}$$

Recall that by representing the reactive flow field with the simplified global reaction containing three species ($N = 3$)

$$1\,\mathrm{F} + \nu\mathrm{Ox} \longrightarrow (\nu^+ 1)\,\mathrm{Pr}$$

we automatically introduce six dependent variables ($2N = 6$): $\dot{m}'''_F(x,y,z,t)$, $\dot{m}'''_{Ox}(x,y,z,t)$, $\dot{m}'''_{Pr}(x,y,z,t)$, $Y_F(x,y,z,t)$, $Y_{Ox}(x,y,z,t)$, $Y_{Pr}(x,y,z,t)$, where we put in evidence the three spatial dimensions and time (the independent variables). The resolving equations are: three species conservation Equation (4.10), one for each species; two mass balances Eq. (4.12) and Eq. (4.13); and one reaction rate Equation (4.14).

[5]Recall that $\frac{D}{Dt} \equiv \frac{\partial}{\partial t} + (\mathbf{V} \cdot \nabla)$.

Relationship between continuity equation and species conservation

Observe that if we sum Equation (4.11) for all N species, we end up with the continuity equation (4.1). The sum of left-hand side (the source term due to chemical reactions), $\sum_{i=1}^{N} \dot{m}_i''' = \dot{m}'''$, results in the total mass created by chemical reaction which is null ($\dot{m}''' \equiv 0$). The first term on the right-hand side contains the derivative of ρ_i which can be expressed as ρY_i that summed for the N species results: $\sum_{i=1}^{N} \rho Y_i = \rho \sum_{i=1}^{N} Y_i = \rho$; while the second term in the right-hand side contains the divergent of $(\rho_i \mathbf{V}_i)$ which can be expressed as $[(\rho \mathbf{V})Y_i]$ that summed for the N species results: $\sum_{i=1}^{N}[(\rho \mathbf{V})Y_i] = (\rho \mathbf{V})$. Organizing the terms, we have equation (4.1).

4.1.2 The Momentum Equation

Newton's second law $\mathbf{F} = m\mathbf{a}$ applies to systems of fixed mass, i.e. particles moving with the flow field. Considering that the forces that act of the particle are body forces (which per unit mass is denoted as $\mathbf{f} = f_x\mathbf{i} + f_y\mathbf{j} + f_z\mathbf{k}$) and surface forces which are due to pressure p or viscous stresses (that in turn subdivide in normal (τ_{ii}) and shear — tangential — stresses τ_{ij}, with $i \neq j$), the Newton second law is called momentum equation and can be written for each coordinate, x, y, z, (using the Cartesian system for simplicity) respectively as:

$$\begin{aligned}
\rho\frac{Du}{Dt} &= -\frac{\partial p}{\partial x} + \frac{\partial \tau_{xx}}{\partial x} + \frac{\partial \tau_{yx}}{\partial y} + \frac{\partial \tau_{zx}}{\partial z} + \rho f_x \\
\rho\frac{Dv}{Dt} &= -\frac{\partial p}{\partial y} + \frac{\partial \tau_{xy}}{\partial x} + \frac{\partial \tau_{yy}}{\partial y} + \frac{\partial \tau_{zy}}{\partial z} + \rho f_y \\
\rho\frac{Dw}{Dt} &= -\frac{\partial p}{\partial z} + \frac{\partial \tau_{xz}}{\partial x} + \frac{\partial \tau_{yz}}{\partial y} + \frac{\partial \tau_{zz}}{\partial z} + \rho f_z
\end{aligned}$$

Upon considering the development of the total derivative, these equations can be rewritten for an infinitesimal control volume fixed in space (Euler framework). Making use of Continuity equation (4.1), the momentum equations become (see Ref.: [16] for details):

$$\frac{\partial(\rho u)}{\partial t} + \nabla(\rho u \mathbf{V}) = -\frac{\partial p}{\partial x} + \frac{\partial \tau_{xx}}{\partial x} + \frac{\partial \tau_{yx}}{\partial y} + \frac{\partial \tau_{zx}}{\partial z} + \rho f_x \tag{4.16a}$$

$$\frac{\partial(\rho v)}{\partial t} + \nabla(\rho v \mathbf{V}) = -\frac{\partial p}{\partial y} + \frac{\partial \tau_{xy}}{\partial x} + \frac{\partial \tau_{yy}}{\partial y} + \frac{\partial \tau_{zy}}{\partial z} + \rho f_y \tag{4.16b}$$

$$\frac{\partial(\rho w)}{\partial t} + \nabla(\rho w \mathbf{V}) = -\frac{\partial p}{\partial z} + \frac{\partial \tau_{xz}}{\partial x} + \frac{\partial \tau_{yz}}{\partial y} + \frac{\partial \tau_{zz}}{\partial z} + \rho f_z \tag{4.16c}$$

In the vast majority of aerodynamic problems, including the reactive flow inside a combustion chamber, the fluids are *newtonian* fluids, i.e. the viscous stress in it is proportional to the time rate of strain. For such fluids, Sir George Gabriel Stokes in 1845 obtained

$$\tau_{xx} = \lambda(\nabla \cdot \mathbf{V}) + 2\mu \frac{\partial u}{\partial x} \tag{4.17a}$$

$$\tau_{yy} = \lambda(\nabla \cdot \mathbf{V}) + 2\mu \frac{\partial v}{\partial y} \tag{4.17b}$$

$$\tau_{zz} = \lambda(\nabla \cdot \mathbf{V}) + 2\mu \frac{\partial w}{\partial z} \tag{4.17c}$$

$$\tau_{xy} = \tau_{yx} = \mu\left(\frac{\partial v}{\partial x} + \frac{\partial u}{\partial y}\right) \tag{4.17d}$$

$$\tau_{yz} = \tau_{zy} = \mu\left(\frac{\partial v}{\partial z} + \frac{\partial w}{\partial y}\right) \tag{4.17e}$$

$$\tau_{xz} = \tau_{zx} = \mu\left(\frac{\partial w}{\partial x} + \frac{\partial u}{\partial z}\right) \tag{4.17f}$$

where μ is the molecular viscosity coefficient (a.k.a. dynamic viscosity) and λ is the second viscosity coefficient. G. Stokes made the hypothesis that

$$\lambda = -\frac{2}{3}\mu \tag{4.18}$$

which is "frequently used but which has still not been definitely confirmed to the present day"[16]. Substituting Eqs. (4.17) into Eqs. (4.16), we obtain the complete Navier-Stokes equations in conservation form:

$$\begin{aligned}\frac{\partial(\rho u)}{\partial t}+\frac{\partial(\rho u^2)}{\partial x}+\frac{\partial(\rho uv)}{\partial y}+\frac{\partial(\rho uw)}{\partial z}&=-\frac{\partial p}{\partial x}\\&+\frac{\partial}{\partial x}\Big(\lambda(\nabla\cdot\mathbf{V})+2\mu\frac{\partial u}{\partial x}\Big)+\frac{\partial}{\partial y}\Big[\mu\Big(\frac{\partial v}{\partial x}+\frac{\partial u}{\partial y}\Big)\Big]\\&+\frac{\partial}{\partial z}\Big[\mu\Big(\frac{\partial w}{\partial x}+\frac{\partial u}{\partial z}\Big)\Big]+\rho f_x\end{aligned}\tag{4.19a}$$

$$\begin{aligned}\frac{\partial(\rho v)}{\partial t}+\frac{\partial(\rho uv)}{\partial x}+\frac{\partial(\rho v^2)}{\partial y}+\frac{\partial(\rho vw)}{\partial z}&=-\frac{\partial p}{\partial y}\\&+\frac{\partial}{\partial x}\Big[\mu\Big(\frac{\partial v}{\partial x}+\frac{\partial u}{\partial y}\Big)\Big]+\frac{\partial}{\partial y}\Big(\lambda(\nabla\cdot\mathbf{V})+2\mu\frac{\partial v}{\partial y}\Big)\\&+\frac{\partial}{\partial z}\Big[\mu\Big(\frac{\partial w}{\partial y}+\frac{\partial v}{\partial z}\Big)\Big]+\rho f_y\end{aligned}\tag{4.19b}$$

$$\begin{aligned}\frac{\partial(\rho w)}{\partial t}+\frac{\partial(\rho uw)}{\partial x}+\frac{\partial(\rho vw)}{\partial y}+\frac{\partial(\rho w^2)}{\partial z}&=-\frac{\partial p}{\partial z}\\&+\frac{\partial}{\partial x}\Big[\mu\Big(\frac{\partial w}{\partial x}+\frac{\partial u}{\partial z}\Big)\Big]+\frac{\partial}{\partial y}\Big[\mu\Big(\frac{\partial w}{\partial y}+\frac{\partial v}{\partial z}\Big)\Big]\\&+\frac{\partial}{\partial z}\Big(\lambda(\nabla\cdot\mathbf{V})+2\mu\frac{\partial w}{\partial z}\Big)+\rho f_z\end{aligned}\tag{4.19c}$$

Upon using the Momentum Equation, we introduce pressure p as the fifth dependent variable in our set of equations. Note that the dynamic viscosity μ is a property of the fluid and may depend on mixture composition and local temperature; in other words, it's a parameter not a dependent variable. The only care that should be taken when applying the Navier-Stokes Eqs. (4.19) to reactive flows is this, considering the proper value of μ that is consistent with both composition and temperature.

4.1.3 Energy equation

The fundamental physical principle that "energy is conserved" simply means that the rate of change of energy of a fluid particle is equal to the rate of heat addition plus the rate of work done. When dealing with reacting flows this principle can be described as

$$\rho\frac{Dh}{Dt}=\nabla\cdot(k\nabla T)-\nabla\cdot\sum_{i=1}^{N}\rho_i\mathbf{U_i}h_i-\nabla\mathbf{q_R}+\frac{Dp}{Dt}+\Phi\tag{4.20}$$

or in conservation form, using an infinitesimal control volume fixed in space as

$$\rho\Big(\frac{\partial h}{\partial t}+(\mathbf{V}\cdot\nabla)h\Big)=\nabla\cdot(k\nabla T)-\nabla\cdot\sum_{i=1}^{N}\rho_i\mathbf{U_i}h_i-\nabla\mathbf{q_R}+\Big(\frac{\partial p}{\partial t}+(\mathbf{V}\cdot\nabla)p\Big)+\Phi \quad (4.21)$$

Equation (4.21) states that the time rate of change of absolute enthalpy h in the infinitesimal control volume fixed in space (left-hand side of Eq. (4.21)) is because of:

1. thermal conduction across the surfaces of the control volume, for which:
   - k is the thermal conductivity of the mixture;
   - ∇T is its temperature gradient;
2. transport of energy by diffusion into (or out of) the control volume across its surfaces, for which:
   - $\mathbf{U_i}$ is the diffusion velocity vector of species i, i.e., $\rho_i\mathbf{U_i}$ is the diffusive flux of the species; given by Fick's Law, Equation (4.8);
   - h_i is the absolute enthalpy of species i;
3. radiative energy emitted or absorbed by the element, for which:
   - $\mathbf{q_R}$ is the radiative heat flux (W/m^2) vector[6]
4. rate of work done by pressure forces exerted on the surfaces of the infinitesimal control volume, recall that $\Big(\frac{\partial p}{\partial t}+\mathbf{V}\nabla p\Big)=\frac{Dp}{Dt}$;
5. rate of work done by shear and normal stresses exerted on the surfaces of the infinitesimal control volume, for which Φ is the *dissipation function* and is given by:
   - $\Phi=\tau_{xx}\frac{\partial u}{\partial x}+\tau_{yy}\frac{\partial v}{\partial y}+\tau_{zz}\frac{\partial w}{\partial z}+\tau_{xy}\Big(\frac{\partial u}{\partial y}+\frac{\partial v}{\partial x}\Big)+\tau_{xz}\Big(\frac{\partial u}{\partial z}+\frac{\partial w}{\partial x}\Big)+\tau_{yz}\Big(\frac{\partial v}{\partial z}+\frac{\partial w}{\partial y}\Big)$

We note that Eq. (4.21) include the effects of species diffusion. (For the detailed derivation of the energy equation see Chapter 17 of Ref.: [17]).

Equation (4.21) does not contain an explicit term for the energy exchange because of chemical reactions. This is because h takes into account the enthalpy of

[6]The radiative heat flux $\mathbf{q_R}$ is usually neglected. However it is proportional to the difference of the fourth power of the temperature of the surroundings of the control volume and its temperature. If the divergent of the heat flux is negative then the control volume is being heated.

formation of the species i, $h^{\circ}_{f,i}$, i.e., h is the absolute enthalpy. In this way the energy exchange due to chemical reactions are automatically taken into account. The absolute enthalpy of the mixture, h, is expressed as

$$h = \sum_{i=1}^{N} Y_i h_i$$

where the species absolute enthalpy is given by

$$h_i = h_{i,sens} + h^{\circ}_{f,i}$$

where $h_{i,sens}$ is the species sensible enthalpy relative to $25°C$ and 1 atm. The enthalpy of formation $h^{\circ}_{f,i}$ of species i can be regarded as its enthalpy at the *standard reference state* of $25°C$ and 1 atm (indicated by the superscript $^{\circ}$) due to its chemical composition[7].

If local thermodynamic equilibrium exists, then we can also write the expression for sensible enthalpy (4.22):

$$h_{i,sens} = \int_{25°C}^{T} c_{p,i} dT \tag{4.22}$$

Where the specific heat at constant pressure for species i, $c_{p,i}$ can be regarded as function of temperature T solely, i.e. $c_{p,i} = c_{p,i}(T)$. That's because we are considering the mixture to behave as an ideal gas:

$$\frac{p}{\rho} = RT \tag{4.23}$$

By doing this we relate the absolute enthalpy of the mixture to its temperature.

After the introduction of the Energy Equation (4.21), the number of dependent variables are six plus N: ρ, u, v, w, p, T, Y_1, Y_2, ..., Y_N. We have shown the necessary equations for equating the problem. There are four governing equations: the continuity equation (4.1), three momentum equations (4.19) (one for each coordinate) and the energy equation (4.21). In addition, there are N species conservation equations (4.10) and two constitutive equations, namely, the expression for sensible enthalpy (4.22) and the ideal gas law (4.23). The number of equations provided is equal to the number of dependent variables, in addition the governing equations for reactive viscous flow were shown in its conservative form, this allows for a numerical solution, given that proper boundary conditions are provided.

[7]Stable elements at the standard reference state have zero enthalpy of formation.

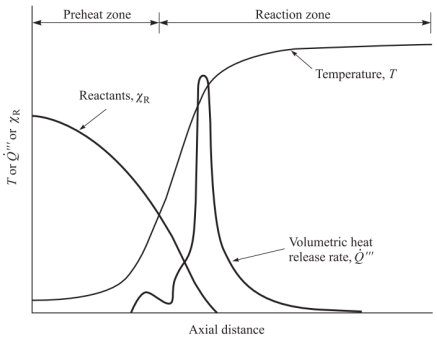

(a) Flame structure: heat release, reactant consumption and temperature trend

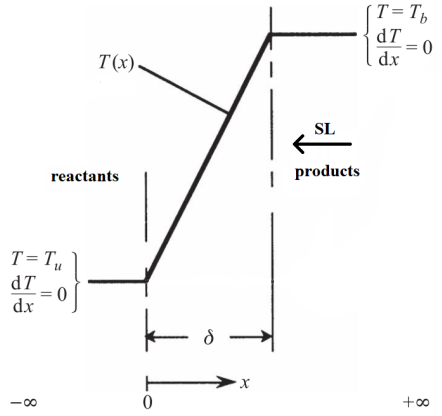

(b) Simplified flame structure: temperature trend

Figure 4.2: Pre-mixed laminar flame structure (Source: adapted from [53])

4.2 Pre-mixed laminar flame - simplified analysis

The pre-mixed laminar flame theory is based on the forementioned mass continuity equation, momentum equation, energy conservation, species conservation, the ideal gas law and the calorific equation (which relates temperature with the enthalpy).

Upon making a series of hypothesis the energy equation can be simplified and after introducing further hypothesis Spalding [1] was able to derive a solution for laminar flame speed and thickness; we'll describe his solution briefly in this section.

Figure 4.2a shows the premixed flame structure. The preheat zone receives heat only through conduction from the reaction zone located downstream where the bulk of chemical reactions occur, i.e. almost no reaction occur in the pre-heat zone. A simplified flame structure (Figure 4.2b) is necessary for we to demonstrate the Spalding solution [1]; it assumes that the temperature profile of the flame is linear and also defines the flame thickness δ in the x region where $^{dT}/_{dx} \neq 0$.

The simplified analysis considers the following assumptions [53]:

1. One-dimensional, constant-area, steady flow;
2. Kinetic and potential energies, viscous shear work, and thermal radiation are all neglected;
3. The small pressure difference across the flame is neglected; thus, the pressure is constant;

4. The diffusion of heat and mass are governed by Fourier's and Fick's laws, respectively. Binary diffusion is assumed;

5. The Lewis number, Le, which expresses the ratio of thermal diffusivity to mass diffusivity, i.e.,

$$Le \coloneqq \frac{\alpha}{\mathcal{D}} = \frac{k}{\rho c_p \mathcal{D}},$$

is unity. This has the result that ${}^{k}/_{c_p} = \rho\mathcal{D}$, which greatly simplifies the energy equation;

6. The mixture specific heat depends neither on temperature nor on the mixture composition. This is equivalent to assuming that the individual species specific heats are all equal and constant;

7. Fuel and oxidizer form products in a single-step exothermic reaction;

8. The oxidizer is present in stoichiometric or excess proportions; thus, the fuel is completely consumed at the flame.

4.2.1 Continuity equation

The assumption 1 can be simply read as the mass flux across the flame is constant, i.e.:

$$\dot{m}'' = \rho c = \rho_u S_L = constant \tag{4.24}$$

which by itself is a representation of continuity equation. The variables ρ and c are the mixture specific mass and mixture velocity, respectively. The subscript u denotes unburned mixture (i.e. fuel and oxidant) and S_L the laminar flame speed.

Species conservation

The simplified analysis of pre-mixed flames assume steady flow for which Equation 4.9 is simplified to

$$\dot{m}_i''' = \frac{\partial}{\partial x}\left[\rho c Y_i - \rho \mathcal{D}_{im} \frac{dY_i}{dx}\right] \tag{4.25}$$

Equation (4.25) is written for each species in the flow: the fuel 'F', the oxidant 'Ox'and the products 'Pr'.

Note that it is possible to relate the species mass production rate $\dot{m}_i'''$ whose unit is given in ${}^{kg}/_{m^3 s}$ and the species mole production rate $\dot{\omega}_i$ given in ${}^{kmol}/_{m^3 s}$ upon multiplying the later by the species molecular weight (MW_i):

$$\dot{m}_i''' = \dot{\omega}_i MW_i \tag{4.26}$$

4.2.2 Momentum equation

Considering that there is no obstructions inside the combustion chamber that may lead to supersonic flow and ultimately in shock waves and no external source of shock waves either, there is no detonation inside the combustion chamber, only deflagration. This implies in little variation of pressure across the flame front such that pressure can be assumed constant; this justifies the assumption 3.

Since we are neglecting viscous forces, and dealing with steady flow the simplified momentum equation $\frac{1}{\rho}dP = cdc$ further simplifies to $dc \approx 0$, meaning that in the course of this Section the momentum conservation equation is not explicitly required.

4.2.3 Energy equation

Spalding bases his solution for flame thickness and speed on a rather simplified form of the energy equation developed by Shvab-Zeldovich. Upon considering the previous assumptions and that a single diffusivity characterizes the mixture the energy equation (4.21) reduces to:

$$\dot{m}'' c_p \frac{dT}{dx} - \frac{d}{dx}\left[(\rho \mathcal{D} c_p \frac{dT}{dx})\right] = -\Sigma h_{f,i}^{\circ} \dot{m}''' \tag{4.27}$$

Which is known as the simplified Shvab-Zeldovich form[8]. It's important to highlight that Eq. (4.21) is the equation solved by numerical techniques in CFD codes during the simulations we are going to show next chapter; the simplified Shvab-Zeldovich form of the energy equation allows for the theoretical solution and in ultimate analysis for a grasp of the underlying physics and dependency of flames on certain mixture parameters.

Equation (4.27) has the physical interpretation that the combined rates of convection (advection) and diffusion of sensible enthalpy (thermal energy) equal the rate at which chemical energy is converted to thermal energy by chemical reaction [53].

[8]The Shvab-Zeldovich form originally considers that mixture specific heat is temperature and composition dependent; the simplified form takes into consideration the assumption 6, i.e. constant c_p.

Observing the simplified global reaction and the resulting mass balance equations (4.12) and (4.13), it's possible to deduce that

$$-\Sigma h^{\circ}_{f,i}\dot{m}''' = \dot{m}'''_F \Delta h_c \tag{4.28}$$

Where Δh_c is the heat of combustion of the fuel.

Because of the unity Lewis number approximation, we also can replace $\rho\mathcal{D}c_p$ with k, the thermal conductivity of the mixture. With these two substitutions, Eq. (4.27) becomes

$$\dot{m}''\frac{dT}{dx} - \frac{1}{c_p}\frac{d\left(k\frac{dT}{dx}\right)}{dx} = -\frac{\dot{m}'''_F \Delta h_c}{c_p} \tag{4.29}$$

4.2.4 Solution

The integration of Eq. (4.29) using the assumed temperature distribution indicated in Fig. 4.2b and subsequently the constant flux condition, Eq. (4.24), together with the relationship between the heat of combustion and temperature increase, $\Delta h_c = (\nu+1)c_p(T_b - T - u)$, yields expressions for the laminar flame speed (S_L) and laminar flame thickness (δ_L) (see [53]):

$$S_L = \left[-2\alpha(\nu+1)\frac{\bar{\dot{m}}'''_F}{\rho_u}\right]^{1/2} \tag{4.30}$$

and

$$\delta = \frac{2\alpha}{S_L} \tag{4.31}$$

Parameters affecting flame speed and thickness It's possible to note from Eq. 4.30 that laminar flame speed S_L is proportional to the square root of thermal diffusivity of the mixture α, the square root of average rate of fuel consumption $\bar{\dot{m}}'''_F$ and the inverse square root of reactants' specific mass ρ_u:

$$S_L \propto (\alpha)^{1/2}(\bar{\dot{m}}'''_F)^{1/2}(\rho_u)^{-1/2}$$

using adequate scales the proportionality translates to[53]

$$S_L \propto (T_u \bar{T}^{0.75} p^{-1})^{1/2}\left[exp\left(-\frac{E_a}{R_u T_b}\right)\left(\frac{p}{T_b}\right)^n\right]^{1/2}\left(\frac{p}{T_u}\right)^{-1/2}$$

where the exponent n is the overall reaction order, and $\bar{T} \equiv 0.5(T_u + T_b)$. With some algebra, such relation simplifies to

$$S_L \propto \bar{T}^{0.375} T_u T_b^{-n/2} exp\Big(- \frac{E_a}{2R_u T_b}\Big) p^{(n-2)/2} \tag{4.32}$$

Equation (4.32) indicates that flame speed has a strong dependence on either unburned gas temperature (T_u) or the burned gas temperature (the adiabatic flame temperature), T_b. It's also affected by the pressure in which combustion takes place; for the case of methane-air mixtures (and also biogas) the overall reaction order is considered $n = 1$, this implies that laminar flame speed S_L decreases with pressure.

However we're more concerned about changes in flame parameters due to fuel change and thus we may focus on how fuel may impact both T_u and T_b. Either a T_u or T_b increase cause the flame speed to increase as well and, as a consequence of Eq. 4.31, flame thickness might decrease in such cases. The opposite is true.

Both flame speed or flame thickness have direct impact on practical flame characteristics: the quenching distance, the minimum ignition energy and the blowout velocity are the most relevant.

The crucial role of methane content in CH_4 - CO_2 mixtures

The parameter of primary interest in a mechanical study regarding the behavior of a MGT and in particular the effects on the combustor when fuel is changed is the percentage of methane in CH_4 - CO_2 mixtures; the biogas being such a mixture with CH_4 percentage ranging from 50 to 60%. It's common practice to say that the biogas has high quality if $\%CH_4$ is high, and that is has low quality otherwise.

The content of methane in the mixture may affect the specific heat ratio slightly and as a consequence the fuel injection temperature (T_u) reduces very little (in the order of $1°C$) when fuel is shifted from natural gas (99% of methane) to a typical biogas (%60 methane). That allows us to disregard changes in the flame due to variation in T_u.

On the other hand, since biogas contains more inert gas (CO_2) than natural gas, the adiabatic flame temperature T_b reduces considerably. At absolute pressure of 612 kPa [9], with fuel injection temperature of 437.0 K and lean combustion with equivalence ratio of 0.5 and dry air at 527 K, the adiabatic flame temperature of the typical biogas results $T_b = 1600K$; whereas at same conditions except the fuel injection temperature that for the natural gas is 438.5 K (recall that its composition is indicated in Table 6.3), the adiabatic flame temperature results $T_b = 1653K$ [25].

[9] The total pressure at inlet of the combustor for the 1500 kW micro gas turbine.

As a conclusion, since T_b is higher for natural gas than for biogas, the natural gas flame has higher flame speed and lower thickness relative to biogas flame. The practical implications of such fuel change will become clear up next.

4.3 Effects on Quenching distance

The quenching distance basically is the flow passage dimension through which the flame looses heat to the walls and extinguish. The Williams criteria states that[53]

1. Ignition will only occur if enough energy is added to the gas to heat a slab about as thick as a steadily propagating laminar flame to the adiabatic flame temperature;
2. The rate of liberation of heat by chemical reactions inside the slab must approximately balance the rate of heat loss from the slab by thermal conduction.

Applying criterion 2, it's possible to demonstrate that the slab width "d", i.e. the quenching distance can be estimated by

$$d = \frac{2\sqrt{b}\alpha}{S_L} \tag{4.33}$$

or, in terms of δ,

$$d = \sqrt{b}\delta \tag{4.34}$$

where b is a number generally much greater than 2[53]. The temperature and pressure dependencies of the quenching distance can be estimated using Eq. (4.32). As a consequence one can infer that the quenching distance for natural gas is smaller than the quenching distance for biogas since natural gas flame speed is higher. This information can be useful for designing the fuel injector (including the pre-mixing duct and eventual recirculation apparatus air intakes) such that core flame flashback can be avoided as it will be discussed the next chapter.

4.4 Effects on Minimum ignition energy

The minimum ignition energy is the minimum energy required to initiate a flame.

To determine such energy, firstly we need to determine the critical gas-volume radius such that a flame will not propagate if the actual radius is smaller than the critical value; in such a case the volume would loose more heat to the surroundings

than it produces through chemical reaction. That's the consideration of Williams criterion 2 again. Secondly, we consider Williams criterion 1 and calculate the energy necessary to heat a spherical volume of the reactant's mixture with the critical radius from T_u to T_b; that's the minimum ignition energy.

From this approach, the critical radius results

$$R_{crit} = \sqrt{6}\frac{\alpha}{S_L} \tag{4.35}$$

and the minimum ignition enegy:

$$E_{ign} = 61.6p\Big(\frac{c_p}{R_b}\Big)\Big(\frac{T_b - T_u}{T_b}\Big)\Big(\frac{\alpha}{S_L}\Big)^3 \tag{4.36}$$

where the R_b is the gas constant of the burned gases.

The minimum ignition energy for natural gas is smaller than for biogas since natural gas flame speed is relatively higher; Equation (4.36) shows a strong proportionality to S_L^{-3}. Again, this information can be useful for designing the ignition system such that either biogas or natural gas mixtures can be ignited with minor changes in the spark control system.

4.5 Effects on Flame stabilization

A pre-mixed flame can have its shape altered and be anchored at different distances from the injector's tip (lift off) depending mainly on the bulk velocity of reactants and on flame speed (S_L).

Ideally the flame is anchored at the injector's tip, however, since the bulk velocity is usually relatively high, the flame might be anchored downstream the injector's tip in a specific location. In such condition, secondary air from the surroundings enters through the flame and the injector's tip reducing the equivalence ratio locally and therefore the local flame speed (the equivalence ratio alters the adiabatic flame temperature directly), on the other hand, the lift off phenomenon is accompanied by a decrease of heat loss to the injector's tip that in turn increase the flame speed one effect opposes the other and a pre-mixed flame can still be anchored in a lift off condition.

4.5.1 Flame blowout

A problem arises when the lift off height is large enough (due to high bulk velocity) and too much secondary air enters lowering the local flame speed to a condition

where the flame no longer may sustain its anchorage. The large bulk velocity *blows out* the flame.

Blow out (also referred as blow off) might happen when the equivalence ratio of the fuel mixture is moved further from unity or a fuel with relatively high LHV (take as an example natural gas) is substituted with a lower LHV fuel (biogas); both actions diminish the adiabatic flame temperature T_b and consequently reduce the flame speed S_L — see Eq. (4.32). Thus the biogas flame in place of natural gas is more prone to blow out. Therefore, one can infer that the bulk velocity of the reactants' mixture leaving the injector could be regulated to avoid flame blowout, specifically the bulk velocity should be reduced for low LHV fuels, such as biogas. This strategy will be tackled on next chapter where we describe an injector alternative with this regulatory capability.

4.5.2 Flame flashback

Conversely, *flashback* occurs when the flame enters and propagates through the burner tube or port without quenching[53], this can lead to injector damage or even explosion.

The phenomenon happens when the bulk velocity is relatively low, being generally a transient event, occurring as the mixture flow is low relative to the normal operating conditions (conditions that apply during start-up or partial load of a MGT), also when the mixture equivalence ratio is moved close to unity or, in a third case, when a fuel with relatively low LHV (biogas) is substituted with a higher LHV fuel (natural gas); both actions increase the adiabatic flame temperature T_b and consequently increase the flame speed S_L — see Eq. (4.32). Thus the natural gas flame in place of biogas is more prone to flashback. Again, the strategy of regulating the bulk velocity of the reactants' mixture leaving the injector could be adopted in the design of an alternative injector aiming at flashback avoidance.

Such injector could be operated as follows: at start up (or shut down), i.e. when flashback is prone to occur, the fuel should be replaced to a lower LHV fuel (Natural gas > biogas) or, if a lower LHV fuel is not available, the injector should be regulated to allow for an increased bulk velocity; at steady operation (e.g. at the design point) whenever fuel shift is required the injector should be regulated to allow for an increased bulk velocity if shifting is done from biogas to natural gas or regulated to allow for a decreased bulk velocity if shifting is done from natural gas to biogas.

These strategies will be tackled on next chapter where we describe an injector alternative with this regulatory capability.

4.6 Chapter conclusions and more

One can note that due to a reduced adiabatic flame temperature characteristic of biogas (when compared to natural gas), the following effects might be observed in pre-mixed flames: reduction in laminar flame speed, increase in laminar flame thickness. As consequence, biogas flame has increased quenching distance and ignition energy.

Quenching analysis indicate that the flow passages in dual-fuel (or multi-fuel) injectors should be designed to avoid flashback when burning the fuel with the highest flame speed (in our case the natural gas), since it has the smallest quenching distance; this would assure that the other fuel (i.e. biogas) flame, with higher quenching distance would get extinguished in case of flashback.

Flashback and blow off could be controlled using an injector capable of regulating the bulk mixture velocity. Essentially, with such capability, the proper match between bulk velocity and flame speed can be attained whenever (1) power transients occur (start-up, partial load), (2) when the mixture equivalence ratio is moved close to unity or (3) when a fuel is substituted with another. This will be object of investigation of next chapter.

4.6.1 Diffusive flames

If the combustor were designed to allow diffusive flames (for instance pilot flames) and the shift were done from natural gas to biogas, it is possible to draw some interesting conclusions using a rather different theoretical approach.

A diffusive flame with fuel-side CO_2 dilution[10] was observed to show reduced flame temperature and NOx formation [14]; in addition, flame length might reduce as well and flame liftoff height may increase.

A diffusive flame with air-side CO_2 dilution was observed to show reduced flame luminosity (and probably NOx) while flame liftoff height and flame length were observed to increase [7].

The air side dilution could be used in some injector designs to counter-act undesired effects of fuel-side dilution, i.e. the use of biogas. However, the combustor object of the present thesis is designed to operate only with lean pre-mixed flames, and only the effects shown in the previous section are of concern.

[10] Biogas can be considered a CO_2 diluted natural gas.

Chapter 5

Nitrogen oxides formation

5.1 General effects of nitrogen oxides - NOx

Although oxides of nitrogen oxides (NOx) occur in many forms in the atmosphere, they are emitted largely as *nitric oxide* (NO) and *nitrogen dioxide* (NO_2) and only these two forms are subject to regulations [3], [46]. The more important of the two is NO_2, a yellow brown to reddish brown gas. Both NO and NO_2 are major contributors to photochemical smog and cause of tropospheric ozone. NO_2 is also a major contributor to acid rain[26]. In addition, these nitrogen oxides may cause eutrophication of water bodies and have various effects on people, including irritation of eyes, nose, throat and increasing susceptibility to viral infections including influenza which can cause bronchitis and pneumonia [26].

5.2 NO formation in combustion

There are four nitric oxide reaction mechanisms: the fuel-NO mechanism where the nitrogen atom comes from a nitrogen-rich fuel; the thermal-NO mechanism where the nitrogen atom comes from high temperature dissociation of N_2 naturally present in the air, the N_2O-intermediate mechanism (significant in lean-premixed combustion), the prompt-NO mechanism where the nitrogen atom comes from the N_2 naturally present in the air after chemical reaction with the hydrocarbon fuel in a fuel-rich flame zone and the recently discovered NNH-mechanism.

Applicability of NO mechanisms Fuel-NO formation is not a concern in biogas or natural gas burning since its concentration in the fuel is minimum.

Figure 5.1 illustrates the contribution of different NO formation mechanisms in lean ($\phi = 0.6$) pre-mixed methane-air flames taken from [43]. For an operating pressure of 6 atm, the N_2O-mechanism might predominate, as expected the thermal-NO mechanism contribution is the smallest and prompt-NO according to this reference may still play a significant role.

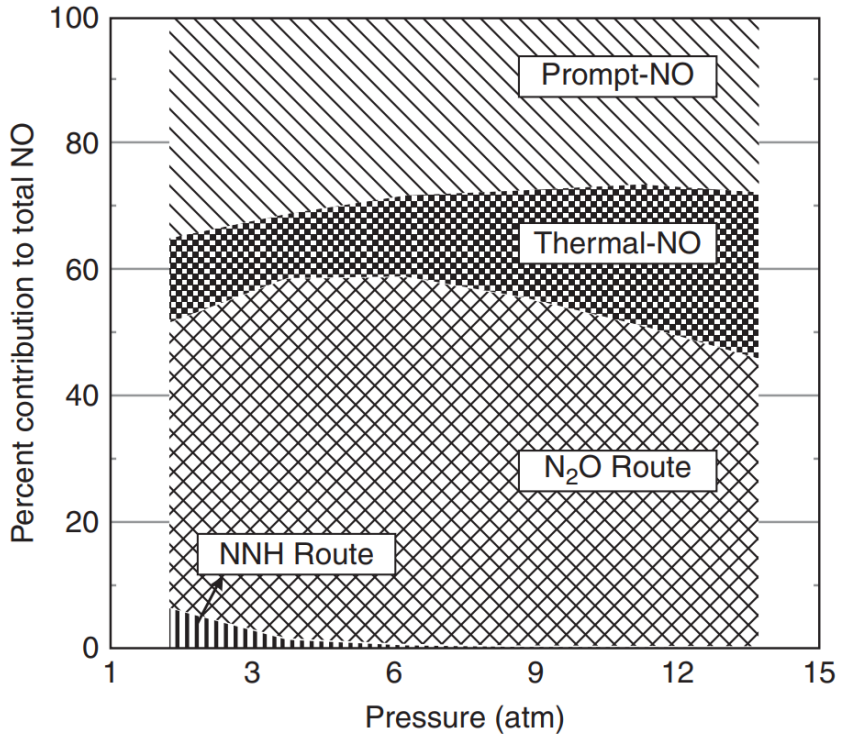

Figure 5.1: Contribution of different NO mechanisms to the total NO as a function of pressure at an equivalence ratio of 0.6 for lean pre-mixed methane-air flames. Source: [43]

Nonetheless, prompt-NO formation was most frequently observed in fuel-rich flames; Glassman describes the prompt-NO mechanism from which the reasons of its increased importance in fuel rich flames could be inferred [37].

In addition, nitric oxide formation by the N_2O-mechanism increases in importance as the air-to-fuel ratio increases (i.e. the equivalence ratio decreases), as the burned gas temperature decreases, or as pressure increases [37],[43].

Figure 5.2 shows that NO formation is independent of pressure for pre-mixed flames with equivalence ratio lower than 0.65. Apparently, NO emissions lower than $2ppm_v$ are hardly obtained.

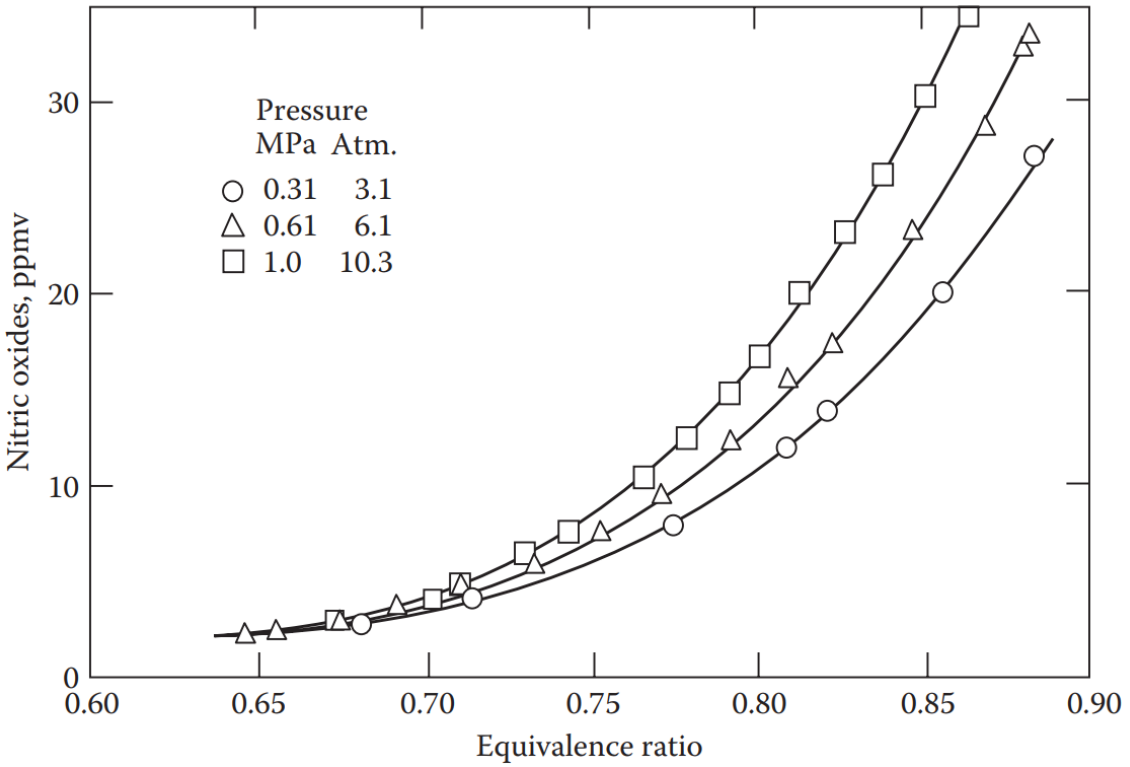

Figure 5.2: Effect of pressure on NO formation. Source: [24]

Up-next we describe the chemical kinetics of thermal-NO and N_2O-intermediate mechanism, the two mechanisms of most concern in the design of the combustor for the 1500 kW MGT using natural gas or biogas. In addition, an overview of the NNH-mechanism is given since recent studies have suggested that it may contribute to as much as 25 to 45% of NO emissions in some specific combustion environments [11].

5.2.1 Thermal-NO mechanism

The thermal-NO mechanism consists in the dissociation and oxidation of molecular nitrogen in the post-flame (where temperature is higher) zone.

The basic mechanism for thermal-NO production is given by six reactions known as *extended Zeldovich mechanism*:

$$O + N_2 \underset{k_{1r}}{\overset{k_{1f}}{\rightleftharpoons}} NO + N \tag{5.1}$$

$$N + O_2 \underset{k_{2r}}{\overset{k_{2f}}{\rightleftharpoons}} NO + O \tag{5.2}$$

$$N + OH \underset{k_{3r}}{\overset{k_{3f}}{\rightleftharpoons}} NO + H \tag{5.3}$$

With reaction rate constants, given by:

$$k_{1f} = 1.8 \cdot 10^{11} e^{-38370/T} \tag{5.4}$$

$$k_{1r} = 3.8 \cdot 10^{10} e^{-425/T} \tag{5.5}$$

$$k_{2f} = 1.8 \cdot 10^{7} \cdot T \cdot e^{-4680/T} \tag{5.6}$$

$$k_{2r} = 3.8 \cdot 10^{6} \cdot T \cdot e^{-20820/T} \tag{5.7}$$

$$k_{3f} = 7.1 \cdot 10^{10} e^{-450/T} \tag{5.8}$$

$$k_{3r} = 1.7 \cdot 10^{11} e^{-24560/T} \tag{5.9}$$

The contribution of reaction (5.3) is small for lean mixtures, but for rich mixtures it should be considered. Forward reaction (5.1) controls the system, but it is slow at low temperatures (high activation energy). Thus it is effective in post-flame zone where temperature is high and residence time is available.

From reactions (5.3) to (5.1), the rate of formation of thermal-NO can be calculated as:

$$\frac{d[NO]}{dt} = k_{1f}[O][N_2] - k_{1r}[NO][N] + k_{2f}[N][O_2] - k_{2r}[NO][O] + k_{3f}[N][OH] - k_{3r}[NO][H] \tag{5.10}$$

To calculate the NO formation rate, we need the concentrations of N, O, OH, and H radicals.

The Quasi-Steady Assumption for [N]

The rate of formation of NO is significant only at high temperatures (greater than 1800 K) because fixation of nitrogen requires the breaking of the strong N_2 triple bond (providing dissociation energy of 941 kJ/mol). This effect is represented by the high activation energy of Reaction 5.1 which makes it the rate-limiting step of the extended Zeldovich mechanism. However, the activation energy for oxidation of N

atoms is small. When there is sufficient oxygen, as in a fuel-lean flame, the rate of consumption of free nitrogen atoms becomes equal to the rate of its formation, and therefore a quasi-steady state can be established. This assumption is valid for most combustion cases, except in extremely fuel-rich combustion conditions [19]. Hence the NO formation rate becomes

$$\frac{d[\mathrm{NO}]}{dt} = 2k_{1f}[\mathrm{O}][\mathrm{N_2}]\frac{1-\frac{k_{1r}k_{2r}[\mathrm{NO}]^2}{k_{1f}[\mathrm{N_2}]k_{2f}[\mathrm{O_2}]}}{1+\frac{k_{1r}[\mathrm{NO}]}{k_{2f}[\mathrm{O_2}]+k_{3f}[\mathrm{OH}]}} \tag{5.11}$$

From Equation 5.11 it is clear that the rate of formation of NO will increase with increasing oxygen concentration. It also appears that thermal NO formation should be highly dependent on temperature but independent of fuel type. In fact, based on the limiting rate described by k_{1f}, the thermal-NO production rate doubles for every 90 K temperature increase beyond 2200 K [19].

Note that after the quasi-steady assumption for [N] the concentration of H radical, [H], does not appear in Equation 5.11.

Partial-equilibrium Assumption for [O]

To solve Equation 5.11, the concentration of O atoms and the free radical OH will be required, in addition to the concentration of stable species (that is, O_2, N_2). Following the suggestion by Zeldovich, the thermal NO formation mechanism can be decoupled from the main combustion process by assuming equilibrium values of temperature, stable species, O atoms, and OH radicals. However, radical concentrations (O atoms in particular) are observed to be more abundant than their equilibrium levels. The effect of partial equilibrium O atoms on NO formation rate has been investigated ([48] apud [19]) during laminar methane-air combustion. The results of these investigations indicate that the level of NO emission can be under-predicted by as much as 28% in the flame zone, when assuming equilibrium O-atom concentrations. Therefore, in our CFD code we set for a NO simulation with partial-equilibrium approach, where the O radical concentration can be expressed as a function of O_2 concentration and temperature [19]:

$$[\mathrm{O}] = 36.64T^{1/2}[\mathrm{O_2}]^{1/2}e^{-27123/T} \tag{5.12}$$

Exclusion of [OH] from thermal-NO calculation

We observe that equation (5.3) in the extended Zeldovich mechanism is much less significant to NO formation than equation (5.2) because:

$$k_{2f}[\mathrm{O_2}]_{eq} \gg k_{3f}[\mathrm{OH}]_{eq} \tag{5.13}$$

which allows us to exclude OH radical from thermal-NO calculation [19]. The simplified NO rate of formation equation is thus:

$$\frac{d[\mathrm{NO}]}{dt} = 2k_{1f}[\mathrm{O}][\mathrm{N_2}]\frac{1-\frac{k_{1r}k_{2r}[\mathrm{NO}]^2}{k_{1f}[\mathrm{N_2}]k_{2f}[\mathrm{O_2}]}}{1+\frac{k_{1r}[\mathrm{NO}]}{k_{2f}[\mathrm{O_2}]}} \tag{5.14}$$

5.2.2 NO Formation from Intermediate N_2O

Melte and Pratt proposed the first intermediate mechanism for NO formation from molecular nitrogen (N_2) via nitrous oxide N_2O, ([45] apud][19]). Nitrogen enters combustion systems mainly as a component of the combustion and dilution air. Under favorable conditions, which are elevated pressures and oxygen-rich conditions (lean-combustion), this intermediate mechanism can contribute as much as 90% of the NO formed during combustion. This makes it particularly important in industrial application such as gas turbines and compression-ignition engines. Because these devices are operated at increasingly low temperatures to prevent NO formation via the thermal NO mechanism, the relative importance of the N_2O-intermediate mechanism is increasing. It has been observed that about 30% of the NO formed in these systems is mainly related to the N_2O-intermediate mechanism [19].

The simplest form of the mechanism shown by Melte and Pratt [45] takes into account two reversible elementary reactions:

$$\mathrm{N_2 + O + M} \underset{\mathrm{k_{1r}}}{\overset{\mathrm{k_{1f}}}{\rightleftharpoons}} \mathrm{N_2O + M} \tag{5.15}$$

$$\mathrm{N_2O + O} \underset{\mathrm{k_{2r}}}{\overset{\mathrm{k_{2f}}}{\rightleftharpoons}} \mathrm{2\,NO} \tag{5.16}$$

With reaction rate constants, given by:

$$k_{1f} = 4.44 \cdot 10^{32} \cdot T^{-8358} \cdot e^{-28234/T} \tag{5.17}$$

$$k_{1r} = 2.90 \cdot 10^{7} e^{-11651/T} \tag{5.18}$$

$$k_{2f} = 4.00 \cdot 10^{8} \cdot e^{-28234/T} \tag{5.19}$$

$$k_{2r} = 1.45 \cdot 10^{-}29 \cdot T^{9259} \cdot e^{-11651/T} \tag{5.20}$$

Here, M is a general third body. Because the first reaction involves the consumption of more gaseous moles than it produces, the mechanism is favored at elevated pressures. In addition, both reactions involve the oxygen radical , which makes the mechanism favored for oxygen-rich conditions. While not always justified, it is often assumed that the radical atoms originate solely from the dissociation of molecular oxygen [19],

$$\frac{1}{2}\mathrm{O}_2 \rightleftharpoons \mathrm{O} \tag{5.21}$$

The rate of NO formation via the N_2O-intermediate mechanism is

$$\frac{d[\mathrm{NO}]}{dt} = 2\Big(k_{2f}[\mathrm{N_2O}][\mathrm{O}] - k_{2r}[\mathrm{NO}]^2\Big) \tag{5.22}$$

Note that to solve Equation (5.22), it's necessary to first calculate [O] and $[N_2O]$.

It is often assumed that N2O is at quasi-steady-state (that is, $^{d[\mathrm{N_2O}]}/_{dt} = 0$), which implies

$$[\mathrm{N_2O}] = \frac{k_{1f}[\mathrm{N_2}][\mathrm{O}][\mathrm{M}] + k_{2r}[\mathrm{NO}]^2}{k_{1r}[\mathrm{M}] + k_{2f}[\mathrm{O}]} \tag{5.23}$$

The system of Equation (5.22) - Equation (5.23) can be solved for the rate of NO formation when the concentrations of N_2, O_2, and M, the kinetic rate constants for Equation (5.15) and Equation (5.16) (see equations (5.17) to (5.20)) and the equilibrium constant of Equation (5.21) (obtained in literature) are known. The appearance of NO in Equation (5.16) entails that coupling of the N2O mechanism with the thermal-NO mechanism (and other NO mechanisms).

5.2.3 NO Formation from NNH-mechanism

This route has been shown to be particularly important in the combustion of hydrogen and for hydrocarbon fuels with large carbon-to-hydrogen ratios [53]. It involves two key reactions:

$$\mathrm{N_2} + \mathrm{H} \longrightarrow \mathrm{NNH} \tag{5.24}$$

$$\mathrm{NNH} + \mathrm{O} \longrightarrow \mathrm{NO} + \mathrm{NH} \tag{5.25}$$

According to [11], this mechanism may apply when fuels are methanol, methane, ethane, ethene, propane, n-butane, and toluene, and carbon-to-hydrogen ratio ranging from 0.25 to 0.88. Methane carbon-to-hydrogen ratio is 0.25, thus this mechanism could be present in the combustion environment of the combustor under

consideration. The rate constant of the second reaction found in [11] is $k = 7 \times 10^{23} cm^3/mol/s$.

5.3 Simulating NO emissions in CFD analysis

Here are some information about how ANSYS Fluent Software models NO emissions.

The ANSYS Fluent software uses rate models developed at the Department of Fuel and Energy at The University of Leeds in England, as well as from the open literature [19].

To predict NO emissions, ANSYS Fluent solves a transport equation for nitric oxide (NO) concentration. When the N_2O-intermediate model is activated, an additional transport equation for N_2O will be solved. The NOx transport equations are solved based on a given flow field and combustion solution. In other words, NO is postprocessed from a combustion simulation. It is therefore evident that an accurate combustion solution becomes a prerequisite of NO prediction. For example, thermal-NOx production doubles for every 90 K temperature increase when the flame temperature is about 2200 K [19]. Great care must be exercised to provide accurate thermophysical data and boundary condition inputs for the combustion model. Appropriate turbulence, chemistry, radiation, and other submodels should be employed.

According to ANSYS Fluent Manual: "to be realistic, one can only expect results to be as accurate as the input data and the selected physical models. Under most circumstances, NOx variation trends can be accurately predicted, but the NOx quantity itself cannot be pinpointed. Accurate prediction of NOx parametric trends can cut down on the number of laboratory tests, allow more design variations to be studied, shorten the design cycle, and reduce product development cost. That is truly the power of the ANSYS Fluent NOx model and, in fact, the power of CFD in general" [19].

In Model 23, during post-processing, the NO formation models were implemented and three mechanisms were considered simultaneously: thermal-NO, N_2O-intermediate and prompt-NO. The results were unsatisfactory since the concentration of NO in the outlet resulted two orders of magnitude lower than 2 ppmv, i.e. the minimum value found in literature. Some hypothesis could be investigated during future simulations in order to model NO formation more realistically:

1. Disregard the prompt-NO mechanism, since [37], [43] and [19] shows that such mechanism is more significant in fuel-rich flames; this approach considers that

the utilization of the prompt-NO mechanism model in a lean pre-mixed flame could lead to unreal results;

2. Use of standard $k - \epsilon$ model in both non-reactive and reactive simulations (instead of using the realizable $k - \epsilon$ model), settting $C_{\epsilon,1} = 1.15$ (instead of the default value 1.44) and $Sc_{turbulent} = 0.2$ (instead of the default value 0.7) in the non-reactive simulations and $C_{\epsilon,1} = 1.30$ and $Sc_{turbulent} = 0.5$ in the reactive simulations. This approach has been adopted in [4] in lean partial pre-mixed methane-air flames whose ultimate research intention was to investigate the correlation between simulated NO formation and experimental data. This strategy would lead to a different reactive flow field that would in turn affect NO formation. In addition, reference [4] makes use of a "partially pre-mixed combustion model" (instead of the reactive volumetric species transport model adopted), if adopted, this also would lead to a different reactive flow field than the obtained;

3. Consider the chemical equilibrium of O radicals (instead of the adopted partial-equilibrium assumption) as adopted by [4];

4. Consider the partial chemical equilibrium of OH radicals (instead of negleting its formation, which is suggested by ANSYS Fluent Manual [19]). This approach was also adopted by [4];

5. Maintain the use of β PDF for temperature modelling in the thermal-NO setup as adopted by [4], i.e. the normal PDF can be disregarded;

6. Possibly, couple the simulation of NO formation, specially to account for the NNH-mechanism to the combustion mechanism, as [53] suggest. It is noted that in post-processing phase only the thermal-NO formation could be accurately simulated, which under 1800 K is negligible. In this case hte turbulence-chemistry interactions might require the Eddy-Dissipation-Concept model, EDC, instead of finite-rate/eddy-dissipation model, see 7.1.2 for details.

Chapter 6

Preliminary design - Reverse Flow Annular Combustor

The basic geometry of any gas turbine combustor is determined mainly by three concerns: first, reduction of total pressure loss that would be excessive if no means of decelerating the flow were provided; second, stabilization of the flame provided by recirculation of hot products; and third, adequate air-to-fuel concentration in the combustion zone.

In our case of combustor for the 100 kW MGT, the first concern is tackled by the use of a diffuser which might be located upstream the air-side of the recuperator, since total pressure loss is also a concern in the design of such device. Therefore, the flow supplied by the recuperator to the combustor has adequate low velocities that may cause reduced total pressure loss. For the combustor to be used in the 1500 kW MGT, the diffuser is located in between the compressor and the combustor inlet, since no recuperator is foreseen in this case.

The third concern is resolved by the use of a liner which allows partial supply of air intake to the combustion zone which is required in lower amounts than the total air provided to the combustor. The remaining air is directed downstream the combustion zone to serve two purposes: cool uniformly the combustion products to levels acceptable by the turbine (dilution air) and cool the liner metal exposed to the combustion zone or persisting hot spots[1] (cooling air).

[1]Hot spots are zones in the liner that are in contact with undesired hot streaks of combustion products, they are predicted to occur in certain zones in the preliminary design of the combustor (curve sections that give access to the turbine) but may be eliminated in the refined design, preferably with very minimal or absence of cooling air directed to these zones.

Combustor layout The layout of the combustor is determined by engine specifications and by the desirability of using wisely the space available. The engine is specified to have a centrifugal compressor and a centripetal turbine connected by an axle that for better mechanical resistance is the shortest as possible. In addition, the flow leaving the compressor and entering the turbine are essentially radial. The combustor layout that best copes with these requirements is the reverse-flow annular combustor.

The centrifugal compressor coupled with a reverse-flow combustor permits the use of a radial diffuser, which is highly efficient with respect to reducing pressure losses in the diffuser and improving flow distribution into the combustor [28]. In addition, the reverse-flow combustor provides a larger combustion volume than would otherwise be obtained with a straight through flow combustion chamber; thus, a potential gain in performance can be realized [28].

Preliminary Desing Steps The preliminary design of the reverse flow annular combustor for the 100 kW recuperated micro gas turbine is the main objective of this chapter, a section is dedicated to the modifications on the preliminary design of the combustor to be arranged in a 1500 kW non-recuperated micro gas turbine.

The preliminary design itself comprises three steps: the first involves the collection and determination of relevant thermodynamic data, the second involves the determination of the main reverse flow combustor dimensions such as casing and liner diameters, liner length, inlet and outlet widths; the third step is carried out after having chosen the liner cooling technologies, and involves the determination of number, diameter and disposition of dilution and cooling holes. To accomplish these steps, it is necessary to have beforehand the flow boundary conditions and the geometrical constrains that the combustor shall respect and a set of correlations based on fluid dynamic parameters, most of them referring to Lefevbre's book Gas Turbine Combustion, Alternative Fuels and Emissions [24]. To determine the main dimensions of the combustor and its preliminary air division, previously than the CFD simulations indicate lack or excess of certain air-flows, data regarding a combustor design with known main dimensions and air division (NASA combustor referred in [28]) were used.

As said, prior to the determination of combustor main dimensions and dimensioning and definition of air passages, the preliminary design involves the collection and determination of relevant thermodynamic data. In the next sections these data are going to be shown and explained in the natural order they are necessary for the design, some calculations are developed in detail in the Appendix A.

First we show the flow boundary conditions and the geometrical constrains that

the combustor shall respect; the combustor design on which we are going to base ours; it is also shown the thermodynamic data regarding the fuel and combustion itself and the preliminary air partitioning in the liner.

Afterwards we describe the determination of the combustor main dimensions and the various air passages to the combustion chamber, the required correlations are going to be explained as they appear.

Figure 6.1 illustrates the recuperated Brayton-Joule cycle in correspondence to the reverse flow combustor for the 100 kW micro gas turbine, its nomenclature will be utilized in this and subsequent sections[2].

The global reaction of combustion between the fuel mixture (valid either for biogases and natural gases) and air is given by:

$$\mathrm{CH_4} + (\tfrac{\chi_{\mathrm{CO_2}}}{\chi_{\mathrm{CH_4}}})\mathrm{CO_2} + (\tfrac{\chi_{\mathrm{N_2}}}{\chi_{\mathrm{CH_4}}})\mathrm{N_2} + \tfrac{2}{\Phi}(\mathrm{O_2} + 3.76\,\mathrm{N_2}) \longrightarrow$$
$$(1 + \tfrac{\chi_{\mathrm{CO_2}}}{\chi_{\mathrm{CH_4}}})\mathrm{CO_2} + 2\,\mathrm{H_2O} + 2\,(\tfrac{1-\Phi}{\Phi})\mathrm{O_2} + (\tfrac{7.52}{\Phi} + \tfrac{\chi_{\mathrm{N_2}}}{\chi_{\mathrm{CH_4}}})\mathrm{N_2}.$$

Molar fractions (χ_i) represent fuel composition and Φ represents the equivalence ratio chosen for operation.

6.1 Geometric constrains, boundary conditions and fuel composition

The geometric constrains and boundary conditions that must be respected and attained by the reverse flow annular combustor for the 100 kW micro gas turbine whose compressor and turbine impellers have been designed at the University of Genoa are presented in Figure 6.2 and Table 6.1. As explained in Chapter 3, the boundary conditions might remain fairly unchanged for the case of natural gas or biogas burning; for the preliminary design we assume they are fixed.

It is opportune to define the fuel composition that are going to be considered in the preliminary design of the reverse flow annular combustor. Table 6.2 shows the Natural Gas composition considered by the literature [32]. For simplicity we consider the Natural Gas composition indicated in Table 6.3, all other fuel gases being accounted for a higher methane molar fraction.

Note however that the preliminary design will based on Natural Gas, as we considered, after analyzing all the fuel cases, that at this stage the variations in the dimensions incurred in the preliminary design due to fuel change are minor.

[2] As reference, one may consider that the isentropic efficiencies of the compressor and turbine for a 100 kW MGT are respectively 0.80 and 0.86, with total-to-total pressure ratios respectively and 4.4 and 3.7.

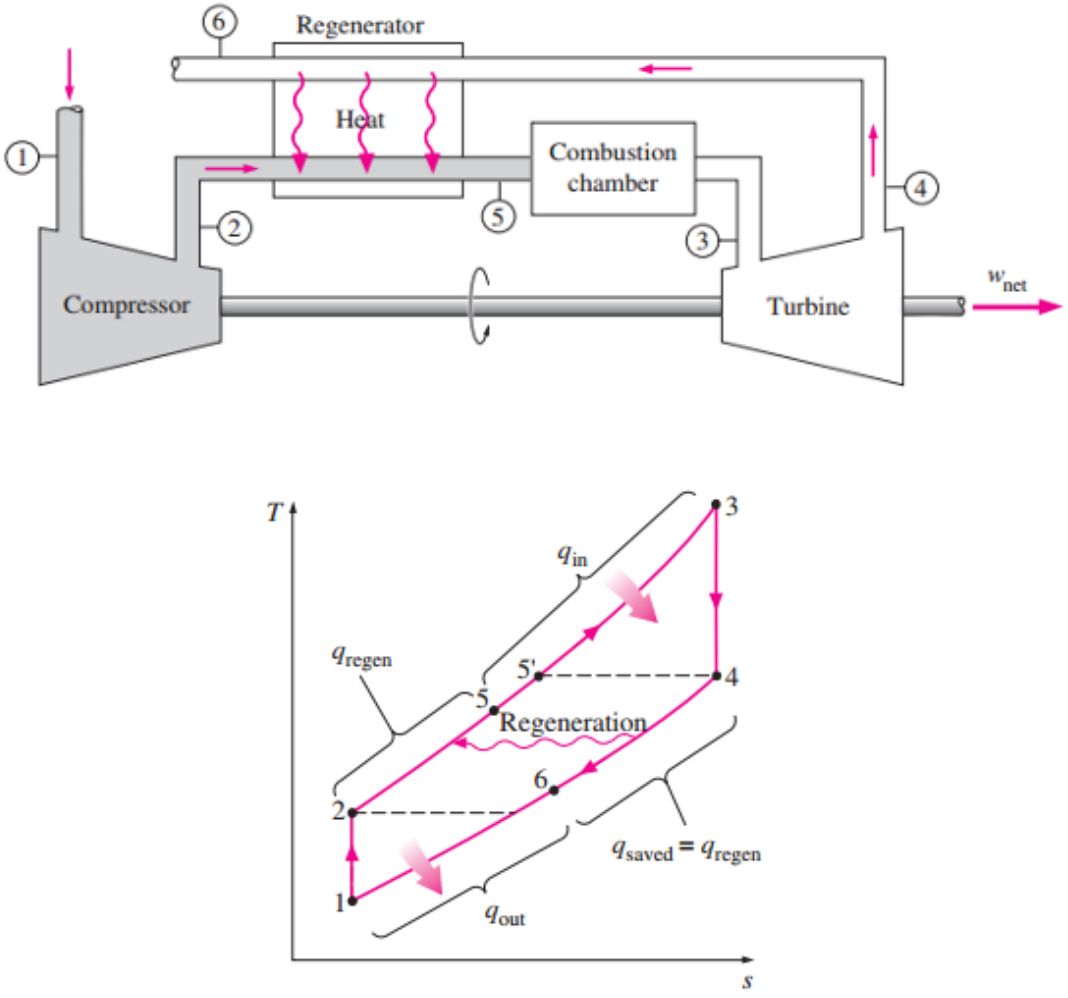

Figure 6.1: Recuperated Brayton-Joule cycle and gas turbine operating on it (Images source: [29])

Table 6.1: Boundary conditions for reverse-flow annular combustor for 100 kW micro gas turbine

Description	**Dimension**	**Unit**
Air mass flow rate '$\dot{m}_1$'	0.72	kg/s
Total temperature at inlet 'T_{05}'	893.15	K
Total pressure at inlet 'P_{05}'	430.00	kPa
Total temperature at outlet 'T_{03}'	1223.15	K

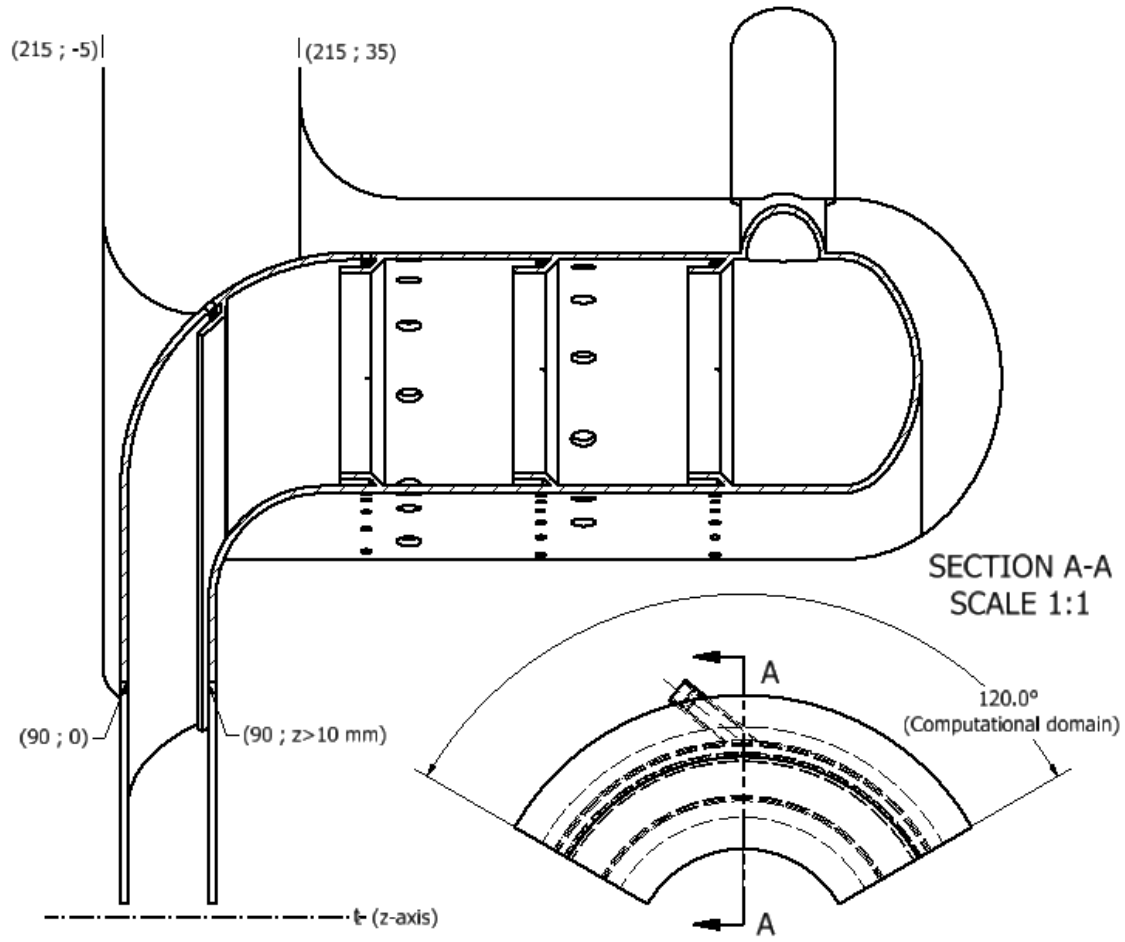

Figure 6.2: Geometric constrains for reverse-flow annular combustor for the 100 kW micro gas turbine

Table 6.2: Natural gas composition indicated by literature [32]

Component	**Molar fraction**
CH_4 (methane)	0.87474
CO_2	0.01181
N_2	0.02648
C_2H_6 (ethane)	0.06332
C_3H_8 (propane)	0.01621
C_4H_{10} (butane)	0.00576
C_5H_{12} (pentane)	0.00168

Table 6.3: Fuel considered in the design of the reverse flow annular combustor: Natural Gas

Component	**Molar fraction**
CH_4 (methane)	0.9902
CO_2	0.0015
N_2	0.0083

6.2 Base design: NASA's reverse flow annular combustor

In 1978, NASA and AVRADCOM[3] used a reverse flow annular combustor suitable for a small gas turbine (2 t o 3 kg/s mass flow) to evaluate the effect of pressure-atomizing fuel injectors density on combustor performance (combustion efficiency, total pressure loss, outlet temperature distribution and liner temperature) and emissions (concentration of unburned hydrocarbons, carbon monoxide and nitrogen oxides and smoke number). Their article's summary of results evidence the possibility to have acceptable performance and emissions while operating with half fuel injector density (9 of 18 fuel injectors were operative) when operating at idle conditions. Operating with all fuel injectors in idle conditions caused flame blowout due to low fuel injector pressure [28].

Despite the fact that their combustor used simplex pressure-atomizing injectors of kerosene Jet-A[4], requiring additional times for atomization, evaporation and mixing which in turn requires designs with longer combustion zones than would be required if natural gas were used (neither atomization nor evaporation or mixing are required in lean pre-mixed natural gas fed combustors as in our case), their combustor was chosen for the base design of ours. As can be inferred, basing our design with injectors for gaseous fuels on theirs would yield conservative results, i.e. longer combustion zones than actually necessary. However, as is going to be shown later, the liner length will be chosen independently to NASA scaling in order to allow a more compact combustor chamber and the combustion zone region will be defined according to recommended Design Practices. Their article provides the whole set of boundary conditions in the design point (Table 6.4), the combustor main dimensions (Figure 6.3 and Table6.5) and the air division in the combustion, dilution and cooling zones (Table 6.6). In addition, the adoption of an even injector number could allow, after the combustor has been constructed, similar performance and emissions testing

[3]AVRADCOM stands for Aviation Research & Development Command (US Army).

[4]The molecular formula of kerosene Jet-A is $C_{13}H_{27}$ ([30]).

Table 6.4: Boundary conditions for NASA combustor in design point (sea-level take-off) and other operative parameters (Ref.: [28])

Description	**Dimension**	**Unit**
Air mass flow rate	3.63	kg/s
Total temperature at inlet	717	K
Total pressure at inlet	1620	kPa
Fuel-to-combustor air ratio 'f_{NASA}'	0.014	-
Total pressure loss [1]	0.017	-

1 As usual in combustor design, total pressure loss refers to the percentage of inlet total pressure.

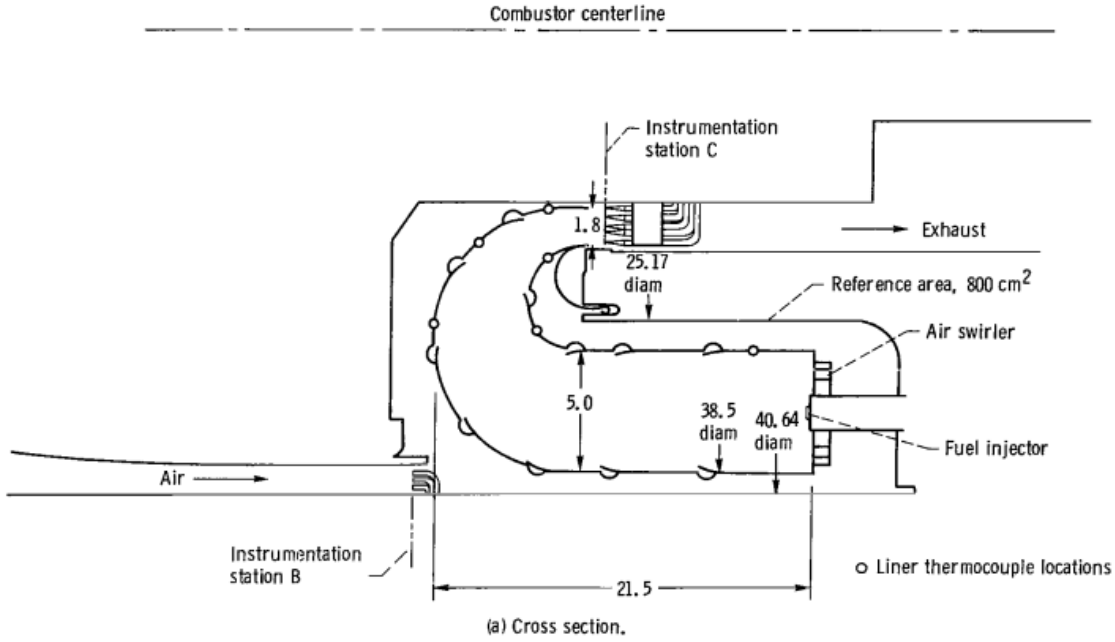

Figure 6.3: NASA combustor with main dimensions (Ref.: [28])

associated with fuel injection density to be carried out.

Table 6.5: Main dimensions of NASA combustor (in centimeters) and derived values (Ref.: [28])

Description	**Dimension**	**Unit**
Outer casing diameter	0.4064	m
Outer liner diameter	0.385	m
Inner casing diameter	0.252	m
Combustor outlet width	0.018	m
Liner overall lenght	0.215	m
Liner height 'H_l'	0.050	m
Reference area [1]	0.08	m^2
Number of injectors	18	-
Directly derived values and dimensions		
Combustor mean diameter	0.335	m
Inner liner diameter	0.285	m
Injectors pitch 'b'	0.058	m
Hl/b ratio	0.86	-
Liner area	0.0526	m^2

1 By definition the reference area of a combustor is the area comprised by the casings in the section of largest diameter, for the case of annular combustors A_{ref} is the annular area comprised between inner and outer casing.

Table 6.6: Liner airflow distribution of NASA combustor (percent of total mass flow) (Ref.: [28])

Swirler	11.2
Primary holes	24.88
Combustion air fraction (α_{NASA})	36.08
Dilution holes	30.8
Concentric around fuel injector (Dome film cooling)	3.17
Liner cooling (Film cooling)	13.12
Outer curve (Film cooling)	13.84
Inner curve (Film cooling)	3.02

Table 6.7: Basic thermodynamic data

Description	Dimension	Unit
$\dot{m}_1$	0.72	kg/s
R_{air}	0.288	$kJ/kg.K$
$LHV_{\mathrm{CH_4}}$ [1]	50050	kJ/kg
T_{amb}	298.15	K
P_{amb}	101.325	kPa
T_{05}	893.15	K
T_{03}	1223.15	K
$c_{p,a}$	1.123	$kJ/kg.K$

1 At standard reference state: 25 °C and 1atm.

6.3 Thermodynamic data regarding the fuel and combustion

6.3.1 Basic data

The basic data to start the composition of the preliminary design thermodynamic data sheet is the total air mass flow rate '$\dot{m}_1$', the gas constant of air 'R_{air}' [5], the lower heating value of methane in the standard reference state, the ambient temperature and pressure, the temperature of air entering the combustor 'T_{05}' and the temperature of gases leaving it 'T_{03}' (see Table 6.7). The specific heat[6] of air at combustor inlet temperature '$c_{p,a}$' comes as a result from these basic data after performing a mole weighted average of specific heats of dry air constituents calculated at combustor inlet temperature (using fourth order polynomials found in literature [29]).

6.3.2 Lower Heating Value of the fuel

The fuel composition is specified by indicating the molar fraction of its constituents (see Table 6.3). After knowing the composition it's possible to determine the lower heating value of the fuel, as better explained in the Appendix section A.1.1, its

[5] Known after the determination of molecular weight of dry air. The air entering the combustor is assumed to be dry air with the composition: 21% O_2 and 79% N_2 which yields molecular weight of 28.840 g/mol.

[6] The combustion chamber is a steady flow device, for this reason the specific heats used in this document all refer to specific heat at constant pressure, in distinction to specific heat at constant volume.

Table 6.8: Fuel data, Natural Gas

Description	Dimension	Unit
LHV [1]	49127	$kJ/kg.K$
MW_f	16.18	g/mol
R_f	0.514	$kJ/kg.K$

1 At standard reference state.

Table 6.9: Fuel injection conditions, Natural Gas

Description	Dimension	Unit
$c_{p,f}$	2.577	$kJ/kg.K$
γ_f	1.277	
T_{inj}	408.82	K
ρ_f	2.071	kg/m^3

molecular weight and its gas constant, as shown by the procedure in the Appendix section A.1.2 and summarized in Table 6.8 for the case of Natural Gas.

6.3.3 Fuel injection conditions

Knowledge about the fuel composition and its molecular weight is essential when determining its specific heat at both ambient temperature and injection temperature, the procedure involves a mole weighted average. However the injection temperature depends on the compression process that in turn depends on the specific heat ratio, function of specific heat and fuel gas constant.

The solution can only be obtained by iterative steps. The specific heat ratio that would better approximate the compression process and that is used in the isentropic compression formula (6.1) for determination of injection temperature, is given by the arithmetic average of the specific heat ratio at ambient temperature and the specific heat ratio at the injection temperature. In this phase we have assumed that the fuel is compressed isentropically in the boosting system up to the injection pressure of 435000 Pa (ambient pressure is assumed 101325 Pa), a value slightly above the total pressure estimated inside the combustion chamber ($P_{03} = 417100Pa$). Results (including the specific mass of fuel at the injection temperature) are summarized in Table 6.9. More details are presented in Section A.1.3.

$$T_{inj} = 298.15 \times 4.29^{\left(\frac{\gamma_f - 1}{\gamma_f}\right)} \tag{6.1}$$

6.3.4 Energy balance in the combustion chamber

Performing an energy balance in the combustion chamber, and to be more precise, including the contribution of sensible heat provided by the fuel to the combustion chamber, the fuel-to-combustor air ratio (f) is determined to be 0.0096. In the preliminary design phase, the combustion efficiency can be assumed to be 100%, such that $f = f_{actual} = 0.0096$. Therefore , the mass flow rate of fuel in nominal conditions results $\dot{m}_f = 0.0096 \times 0.72 = kg/s$ for Natural Gas combustion; more details are given in Section A.2.

6.3.5 Lean premixed flame in combustion zone

It is desired that in nominal conditions the combustor operate with a stable lean premixed flame. For this purpose, the equivalence ratio chosen when burning natural gas is 0.5 in the preliminary design, and allowed to raise up to 0.55 if necessary in the design refinement. Section A.3 details the determination of the air-to-fuel ratio (AFR) to be used in the combustion zone to respect the equivalence ratio chosen. It details also the determination of the combustion air fraction (α) which orients the amount of air that must pass through the injectors to sustain the lean combustion zone. It results that $AFR = 33.60$ and $\alpha = 0.319$ for Natural gas combustion.

6.4 Preliminary air partitioning in the liner

As explained earlier, the function of the liner is to allow the division of air flow to the different zones in the combustion chamber. Since we are basing our design on the design presented by NASA [28], the air partitioning (Table 6.10) will be based on Table 6.6. Such air partitioning is independent on fuel choice. Due to the absence of primary holes in our design and since the combustor we are designing does not allow combustion zones with different equivalence ratio (lean combustion with equivalence ratio 0.5 is desired throughout the combustion zone) all combustion air will enter through the swirlers to sustain a lean pre-mixed flame, this fraction is set equal to the combustion air fraction (α). In addition, The dome cooling flow rate is included in the liner cooling flow since in the design for the 100 kW MGT combustor the dome is not in contact with the flame. The remaining air $(1 - \alpha)$ is split among the other passages according to the contribution each passage had relative to the sum of all other fractions in the NASA design, excluding the combustion air fraction, for example,

Table 6.10: Preliminary liner airflow distribution of the reverse flow combustor (percent of total mass flow)

Swirler	31.9
Primary holes	-
Combustion air fraction (α)	31.9
Dilution holes	32.8
Concentric around fuel injector (Dome film cooling)	-
Liner cooling (Film cooling)	17.4
Outer curve (Film cooling)	14.7
Inner curve (Film cooling)	3.2

Table 6.11: Preliminary mass flow rates through liner (in kg/s)

Swirlers	0.230
per swirler	0.077
Dilution holes	0.236
Concentric around fuel injector (Dome film cooling)	-
Liner cooling (Film cooling)	0.125
Outer curve (Film cooling)	0.106
Inner curve (Film cooling)	0.023
Total	0.72

$$Y_{Dil} = (1 - \alpha) \times \frac{Y_{Dil,NASA}}{(1 - \alpha_{NASA})} \tag{6.2}$$

where Y_{Dil} stands for the dilution air fraction.

Multiplying these fractions by the air mass flow rate of $0.72\,\mathrm{kg\,s^{-1}}$ indicated in Table 6.1, the preliminary mass flow rates preliminary in each zone can be determined (Table 6.11). The design of the combustor for the 100 kW MGT will have three swirlers whose outlet flow is mainly tangential to the inner liner.

Figure (6.4) illustrates the preliminary mass flow rates through the liner. Note that half of the dilution air is directed to the inner liner and the other half to the outer liner. The liner contains four film cooling passages, so one fourth of the air is directed to each.

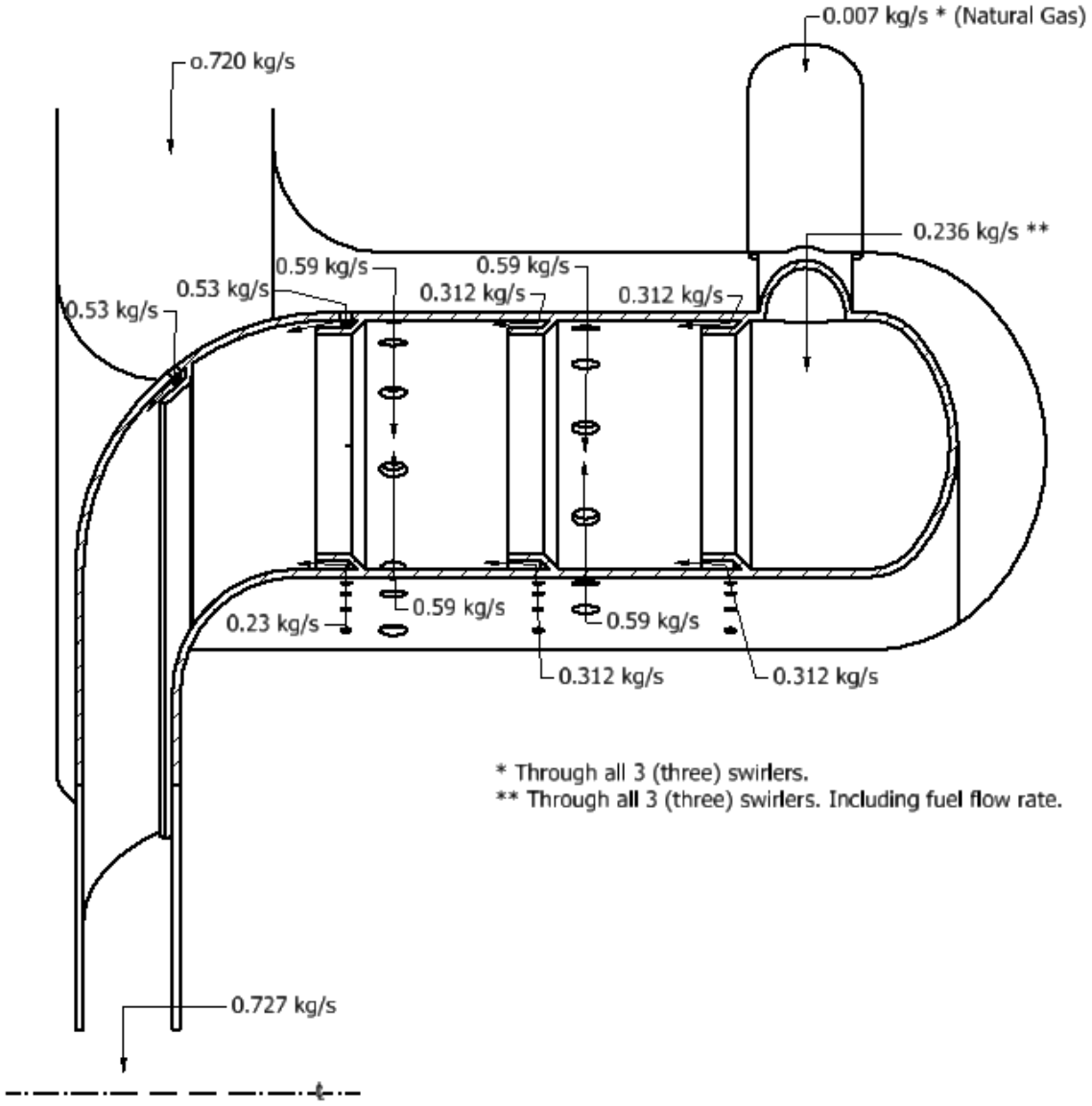

Figure 6.4: Preliminary mass flow rates through liner (in kg/s)

6.5 Scaling procedure using the non-dimensional flow rate

There are two scaling procedures of NASA combustor dimensions (6.3), the first uses the non-dimensional flow rate equality, the second uses the load parameter equality. Since both combustors have the same typology (reverse-flow annular), the first procedure can be adopted and imposes the equality of *non-dimesional mass flow* ($\dot{m}\sqrt{T_0}/_{A_{ref}P_0}$) of NASA combustor and ours.[7]

The square of non-dimensional mass flow is proportional to total pressure loss in the combustion chamber [36] and after imposing the equality we may expect the total pressure loss of our combustor to be similar to NASA's total pressure loss (1.7%), therefore, we impose a value of 1.7% total pressure loss ($^{\Delta P_0}/_{P_{05}}$) resulting in $\Delta P_0 = 7310Pa$. For simplicity in the preliminary design phase, this pressure loss is also assumed to be the same across all passages between the annulus and the combustion chamber, such hypothesis is obviously too restrictive and the subsequent numerical simulations shall indicate total pressure losses that in different locations inside the chamber better correspond to reality.

Using NASA boundary conditions (Table 6.4), reference area (Table 6.5) and our boundary conditions (Table 6.1), imposing the equality mentioned above we obtain the reference area of our combustor to be $0.0667m^2$. We then divide our reference area by NASA's and take the square root to obtain the linear scale factor equal to 0.913.

With respect to the main combustor dimensions there are some Design Practices that are recommended, preferably the combustor scaling might be in accordance with them. In particular it is recommended that:

- The straight liner lenght 'L_c' to liner height 'H_l' be equal to 2.5;
- the lenght of combustion zone, defined between dome extremity and beginning of first liner film cooling exit be equal to 'H_l';
- other recommendations are not imposed but values coming from the scaling procedure are expected to attend closely to them (see notes on Table 6.12).

The scaled main dimensions of NASA combustor are reported in Table 6.12.

[7]The true non-dimensionsal mass flow equation contains the gas constant multiplying the temperature inside the square root, we have dropped it automatically since it is assumed that both combustion chambers receive as intake air with the same composition.

Table 6.12: Main dimensions of reverse combustor (preliminary design)

Description	**Dimension**	**Unit**
Outer casing diameter	0.371	m
Outer liner diameter	0.352	m
Inner casing diameter	0.230	m
Combustor outlet width	0.016	m
Liner overall lenght[1]	0.162	m
Liner height 'H_l'	0.046	m
Straight liner lenght 'L_c'	0.114	m
Reference area	0.0667	m^2
Directly derived values and dimensions		
Combustor mean diameter	0.306	m
Inner liner diameter	0.260	m
Injectors pitch 'b' [2]	0.053	m
H_l/b ratio [3]	0.86	-
L_c/b ratio [4]	2.138	-
Liner area 'A_{liner}'	0.044	m^2

1 Override from $0.196m$ to allow for a more compact combustor.
2 Design practices recommends b between 2.5 and 3.3 inches, i.e. between 0.0635 and $0.08382m$.
3 Remain equal to the NASA ratio. It should result close to unity.
4 Design practices recommends Lc/b ratio to be larger than 2.5.

In this stage we can calculate also the specific mass of air entering NASA combustor ($\rho_{5,NASA} = 7.837kg/m^3$) where we used ideal gas law considering $R_{air} = 0.288kJ/kg.K$, temperature and pressure indicated in Table 6.4). Using the continuity equation and considering the reference area we can determine their reference velocity ($5.79m/s$) and reference dynamic pressure ($131.5Pa$). The same can be done with our combustor whose results are: $\rho_5 = 1.670kg/m^3$, $v_{ref} = 6.47m/s$, $P_{d,ref} = 34.90Pa$.

6.6 The load parameter θ usage

An alternative scaling procedure would impose the equality of *load parameter* 'θ' of NASA combustor and ours. The load parameter can be given by:

$$\theta = \frac{P_{05}^{1.75} A_{ref} H_l e^{(T_{05}/b)}}{\dot{m}_1}$$

where boundary conditions, reference area and liner height might be used. In addition, 'b' is the reaction rate parameter that is a function of equivalence ratio in the combustion zone.

In combustion systems where fuel evaporation and mixing rates occur relatively much faster than chemical reactions (reaction-controlled systems) the load parameter correlate well with the combustion efficiency such that imposing equality of load parameter between both combustors means to aim for similar combustion efficiencies. However care should be taken, the combustor we are designing can be considered a reaction-controlled system since it operates with premixed flames of mixtures of methane and carbon dioxide, where it is assumed that neither evaporation nor mixing are required. On the other hand, NASA combustor uses simplex injectors with Jet-A kerosene meaning that it requires both evaporation and mixing processes, the load parameter would not correlate well with efficiency in this case. For cases like NASA combustor, it would be more adequate to use criteria for mixing-controlled systems or even evaporation-controlled systems presented in the literature [24].

Notwithstanding, after our combustor has been built and tested, the load parameter could serve for predicting combustion efficiency in off design conditions, since $\eta_b = f(\theta)$. The load parameter uses boundary condition parameters ($\dot{m}_1$, P_{05} and T_{05}) and the reaction rate parameter 'b' that would take into consideration change in equivalence ratio in the variation of combustion efficiency.[8]

6.7 Gas properties estimated inside the liner

It is convenient to individuate three control sections inside the combustion chamber since some properties in them affect the combustor outlet velocity, the estimated static pressure at outlet, quantity and diameter of dilution holes and the estimated liner temperatures (i.e. the evaluation of liner cooling effect). These sections are shown in Figure 6.5 and correspond to: (1) end of combustion zone (before dilution and mixing with cooling films of liner and dome occur; the location of this section is uncertain in the preliminary design phase); (2) beginning of dilution zone (by definition located at the plane of first dilution holes) and (3) combustor outlet.

In control section (1) we need to determine the temperature 'T_{s1}', mass flow rate '$\dot{m}_{s1}$'and specific mass 'ρ_{s1}' to allow the determination of the temperature and velocity of gases entering section (2) 'T_{s2}', 'v_{s2}', respectively.

[8]Some experts might use the load parameter to investigate off-design performance or to scale combustors that operate with the same liquid fuel, even if it is technically considered a mixing-controlled system or evaporation-controlled system.

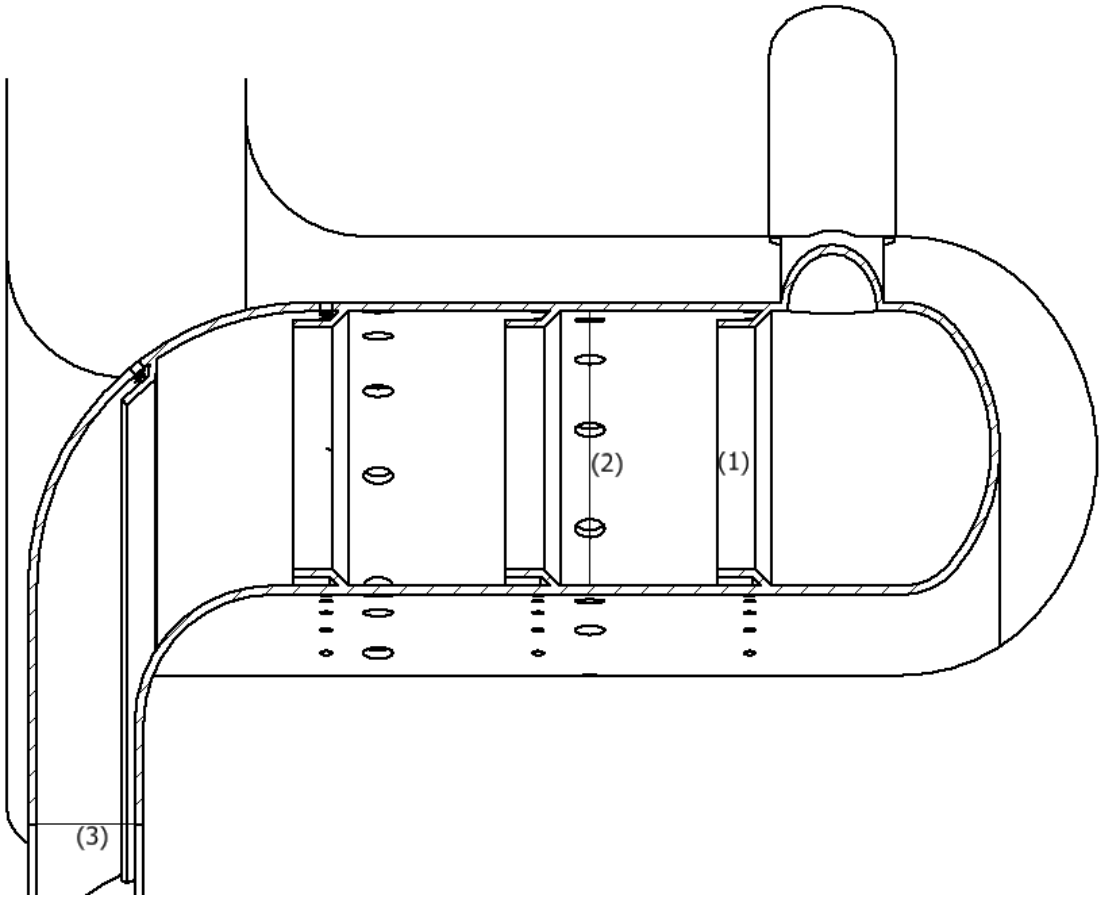

Figure 6.5: Control sections inside combustion chamber

In control section (2), the determination of the gas constant 'R_{s2}' will allow the determination of the specific mass in this section 'ρ_{s2}'.

In control section (3), the mass flow rate of gases, given by the sum of $\dot{m}_1$ and $\dot{m}_f$, and the specific mass ρ_{s3} will determine the combustor outlet velocity (v_{outlet}) and the estimated static pressure (P_3).

6.7.1 Variables at control section (1)

To determine the thermodynamic properties of the products leaving the combustion zone (section 1) some assumptions need to be taken:

- The combustion zone do NOT comprise the cooling flow of dome or liner;

- Combustion is assumed to have 100% efficiency;
- Combustion follows the global reaction given in A.3.

The energy balance in the combustion zone can be solve for 'T_{s1}' ((6.3)), it is required knowledge about: $\dot{m}_1 = 0.72kg/s$, $T_{05} = 893.15K$, $c_{p,a} = 1.123kJ/kg.K$, $LHV = 49127kJ/kg.K$, $c_{p,f} = 2.577kJ/kg.K$, $T_{inj} = 408.82K$, $\dot{m}_f = 0.007kg/s$, $\alpha = 0.319$, mass flow rate of combustion products ($\dot{m}_{s1} = \alpha \times \dot{m}_1 + \dot{m}_f = 0.236kg/s$) and the specific heat of products in this section $c_{p,s1}$ evaluated at T_{s1}, which prompts for an iterative solution, this can be done since the composition of products leaving section (1) can be inferred.

$$T_{s1} = 298 + \frac{\alpha \dot{m}_1 c_{p,a}(T_{05} - 298) + \dot{m}_f c_{p,f}(T_{inj} - 298) + \dot{m}_f LHV}{\dot{m}_{s1} c_{p,s1}} \tag{6.3}$$

The specific heat at molar basis of products leaving section (1) is determined by the mole weighted average of specific heats using the right-hand side of global reaction. The molecular weight of products leaving section (1) is determined by taking the weight of one mole of products, given by the sum of moles of compounds in right-hand side of global reaction multiplied respectively by the molecular weights, and dividing by the number of moles present on the right-hand side of the reaction. The specific heat at mass basis comes from the division of specific heat at molar basis by the molecular weight.

The specific mass at section (1) 'ρ_{s1}' is determined with ideal gas law using 'R_{s1}' (determined after calculation of molecular weight of products in (1)), T_{s1} and total pressure inside the liner '$P_{05} - \Delta P_0 = 422690Pa$.

After the calculations it results that $c_{p,s1} = 1.359kJ/kg.K$, $T_{s1} = 1827K$ and $\rho_{s1} = 0.785kg/m^3$.

Since $\dot{m}_{s1} = 0.236kg/s$, $\rho_{s1} = 0.785kg/m^3$ and $A_{liner} = 0.044m^2$, the mean velocity across section (1) is estimated at $6.83m/s$.

6.7.2 Variables at control section (2)

The temperature of gases entering dilution zone 'T_{s2}' differs from T_{s1} because it is assumed that in (2), the cooling flows of liner and dome have finally mixed with the products leaving the combustion zone. 'T_{s2}' can be estimated with another energy balance (6.4) where the mass flow of combustion products $\dot{m}_{s1} = 0.236kg/s$ (with $c_{p,s1} = 1.359kJ/kg.K$ at $T_{s1} = 1827K$) mixes with half the mass flow of liner cooling ($\dot{m}_{film} = \frac{0.125}{2} = 0.625kg/s$ according to Table 6.11) whose temperature is

$T_{05} = 893.15K$ and specific heat $c_{p,a} = 1.123kJ/kg.K$. The specific heat at section (2) $c_{p,s2}$ is determined by knowledge on composition and mass flow rate of streams and a mass weighted average.

$$\dot{m}_{s1}c_{p,s1}(T_{s1} - 298) + \dot{m}_{film}c_{p,a}(T_{05} - 298) = \dot{m}_{s2}c_{p,s2}(T_{s2} - 298) \tag{6.4}$$

After determining, $c_{p,s2} = 1.310kJ/kg.K$ and solving the energy balance (where $\dot{m}_{s2} = \dot{m}_{s1} + \dot{m}_{film} = 0.299kg/s$) for T_{s2} results $1659K$.

The knowledge on composition and mass flow rate of film cooling and products from section (1) allows the determination of molecular weight in section (2) $MW_{s2} = 28.332g/mol$, then the gas constant $R_{s2} = 0.293kJ/kg.K$.

The specific mass at section (2) 'ρ_{s2}' is determined with ideal gas law using 'R_{s2}', T_{s2} and total pressure inside the liner ($P_{05} - \Delta P_0 = 422690Pa$) to be $\rho_{s2} = 0.868kg/m^3$.

The velocity of gases entering section (2) is determined by continuity to be $v_{s2} = {}^{\dot{m}_{s2}}/_{\rho_{s2}A_{liner}} = 7.846m/s$.

6.7.3 Variables at control section (3)

The mass flow rate of exhaust products is the sum of fuel and total air flow rate: '$\dot{m}_{s3} = 0.727kg/s$'.

The total mole flow rate leaving combustor can be calculated as explained in Section A.4 to be $25.392mol/s$, since we know the mass flow rate of exhaust products, the molecular weight of exhaust products leaving the combustor and reaching the turbine can be determined by division to be $28.627g/mol$ to which corresponds the gas constant $R_{s3} = 0.290kJ/kg.K$.

The specific mass at combustor outlet 'ρ_{s3}' is determined with ideal gas law using 'R_{s3}', T_{03} and total pressure inside the liner ($P_{05} - \Delta P_0 = 422690Pa$) to be $\rho_{s3} = 1.190kg/m^3$.

The outlet combustor area calculated is given by $A_{outlet} = (2\pi 0.090) \times 0.0164 = 0.0093m^2$, after observation of outlet radius in Figure 6.2 and outlet width in table 6.12. The estimated combustor outlet velocity 'v_{s3}' is determined by continuity to be $v_{s3} = v_{outlet} = {}^{\dot{m}_{s3}}/_{\rho_{s3}A_{outlet}} = 65.72m/s$.

From the outlet velocity and specific mass, it's possible to calculate the outlet dynamic pressure: $P_{d,s3} = {}^{\rho_{s3}v_{s3}^2}/_2 = 2.57kPa$ and by subtraction from the total pressure inside the liner ($P_03 = 417.10kPa$), given the subsonic nature of the flow field, the estimated static pressure at outlet $P_3 = 420.12kPa$.

Before passing to the determination of liner flow passages (swirler, fuel injection holes, dilution holes and cooling flows), we clarify that the specific heat of exhaust

gases $c_{p,g} = c_{p,s3} = 1.224kJ/kg.K$ was necessary above in the energy balance for the determination of the fuel-to-combustor air ratio ($f = 0.0096$), which allowed the determination of fuel flow rate that, in turn, contributed to the mass flow rate of exhaust products '$\dot{m}_{s3} = 0.727kg/s$' and determined the estimated composition of gases inside the liner various sections (1,2,3). The determination of $c_{p,s3}$ was possible only through an iterative process whose gases composition and flow rate in section (3) were considered.

6.8 Dilution holes quantity and diameter

6.8.1 Number of dilution holes

The definition of number of dilution holes uses the Cranfield design method (shown in [24]) and start by the choice of maximum penetration of dilution air jets 'Υ_{max}' which is arbitrarily expected to be 72% of H_l, the local liner height[9]. Therefore, $\Upsilon_{max} = 0.72 \times 0.046 = 0.033m$. The momentum flux ratio of dilution jet to liner stream J is also required to proceed with the correlations:

$$J = \frac{\rho_5 \cdot v_{across,liner}^2}{\rho_{s2} \cdot v_{s2}^2} \tag{6.5}$$

Using our data, J results 268.62.

The jet effective diameter 'd_j' is obtained with the correlation (6.6) shown in literature [24] for penetration of multiple jets where the coefficient 1.25 is replaced by 1.05 a modification that better apply to reverse flow combustors:

$$d_j = \frac{\Upsilon_{max} \cdot (\dot{m}_{s2} + \dot{m}_{dilution})}{1.05 \cdot \sqrt{J} \cdot \dot{m}_{s2}} \tag{6.6}$$

Where $\dot{m}_{dilution}$ is the preliminary mass flow rate of dilution jets and is given in Table 6.11 to be equal to $0.235kg/s$.

After performing the calculations d_j results $3.1mm$.

The number of dilution jets follows Cranfield correlation (6.7):

$$n_{dilution} = 15.25 \cdot \dot{m}_{dilution} \cdot ({}^{P_{05}\Delta P_0}/_{T_{05}})^{-0.5} \cdot d_j^{-2} \tag{6.7}$$

Note that the $n_{dilution}$ decreases with an increase of maximum penetration of dilution air jets Υ_{max} since this causes the jet effective diameter d_j to increase. After performing the calculations with our data, it results that $n_{dilution} = 192$ holes,

[9]It is advised that dilution jets penetrate more than 50% the liner height.

distributed equally in four (4) rows, two at inner liner and two at outer liner, makes up for 48 holes per dilution row. [10].

6.8.2 Diameter of dilution holes

The diameter of dilution holes differs from inner and outer liner sides. This is due to the evident facility the dilution air penetrate the outer liner. It is expected that the discharge coefficient for these rows result higher than for inner rows.

The discharge coefficient of a hole through a liner wall where there is flow in the annulus parallel to the plane of the hole is given by the correlation (6.8) ([39] apud [24]):

$$C_d = \frac{1.25(K-1)}{[4K^2 - K(2-\alpha')^2]^{0.5}} \tag{6.8}$$

The variable 'α'' is the ratio of hole mass flow rate to annulus mass flow rate. For the inner annulus:

$$\alpha' = {}^{\dot{m}_{dilution}}/_{\dot{m}_{inner,annulus}}.$$

The quantity $\dot{m}_{inner,annulus}$ refers to the mass flow rate in the inner annulus before entering the dilution zone, in this position of the annulus it is presumed that all air has entered the combustion chamber, except for the inner curve cooling air ($\dot{m}_{cool,inner,curve} = 0.023kg/s$) and half of dilution air (${}^{\dot{m}_{dilution}}/_2 = 0.118kg/s$), resulting in $\dot{m}_{inner,annulus} = 0.141kg/s$. Under these conditions, α' results 1.672.

Variable 'K' is the ratio of the jet dynamic pressure to the annulus dynamic pressure upstream of the holes (a.k.a. hole pressure loss factor):

$$K = \frac{v^2_{across,liner}}{v^2_{inner,annulus}}$$

The velocity $v_{inner,annulus}$ is determined from knowledge of inner annulus area $A_{inner,annulus}$ obtained from the scaled dimensions (Table 6.12) to be $0.0117m^2$. Using the continuity equation and considering $\rho_5 = 1.670kg/m^3$ and $\dot{m}_{inner,annulus} = 0.141kg/s$ it results that $v_{inner,annulus} = 7.18m/s$. K results 169.63. Equation (6.8) gives $C_{d,inner,dilution} = 0.621$.

[10] For numerical simulation purposes it is desirable to analyze a section of the combustor and impose periodic boundary conditions, this can be done if the number of holes per dilution row (and other flows) are a multiple of number of swirlers , i.e. multiple of three (3).

Flow conditions leading to dilution jets in the outer liner are similar to those in the inner annulus; for preliminary design purposes, we stipulate that the discharge coefficient in the outer liner is equal to that in the inner liner.

According to [24], the actual geometric diameter of the dilution holes is given by the correlation (6.9):

$$d_h = {}^{d_j}/_{C_d^{0.5}} \tag{6.9}$$

From which the dilution diameters result after round up: $d_h = 4mm$.

6.9 Cooling flows

The preliminary design of cooling passages assumes that the amount of cooling air indicated in Table 6.11 is enough to avoid hotspots in the liner and curve sections.

After having decided for the utilization of splash-cooling rings for liner and curve sections cooling. The determination of quantity and diameter of respective cooling holes is straightforward after a discharge coefficient of 0.7 is arbitrarily associated with the splash-cooling rings.

The theoretical discharge is calculated by $\rho_5 A_{holes}(2\Delta P_0/\rho 5)$. The actual discharge is given in Table 6.11. The diameter of holes are chosen in order to attain multiplicity with number of injectors[10].

After having chosen holes with 2 mm diameter, the liner results to have 90 holes for each of its four cooling rings; the outer curve results to have 153 holes for each of its two cooling rings and the inner curve results to have 66 holes in its single cooling ring.

6.10 Preliminary design modifications concerning the combustor for the 1500 kW MGT

The shown methodology used in the preliminary design for the 100 kW MGT combustor applies also for the preliminary design of the 1500 kW MGT combustor whose boundary conditions are indicated in Table 6.13.

The preliminary design of the 1500 kW MGT combustor required the following modifications and remarks to be applied:

- Differently than the 100 kW MGT combustor, whose injectors in the preliminary configuration will be set tangentially with respect to the inner liner, the

Table 6.13: Boundary conditions for reverse-flow annular combustor for 1500 kW micro gas turbine

Description	**Dimension**	**Unit**
Air mass flow rate '$\dot{m}_1$'	7.48	kg/s
Total temperature at inlet 'T_{05}'	527.00	K
Total pressure at inlet 'P_{05}'	612.00	kPa
Total temperature at outlet 'T_{03}'	1223.15	K

injectors for the 1500 kW MGT in the preliminary design will be located axially with respect to the liner. This in turn requires the dome to be cooled. After the first CFD simulations, the injector mounting typology, tangentially or axially, will be varied either for the 100 kW MGT combustor and the 1500 kW MGT combustor in order to assess the differences in the flow patterns created.

- The combustor for the 1500 kW MGT does not have a recuperator, so the inlet connects directly to the diffuser downstream the compressor. The inlet passes from being radial as in the 100 kW MGT combustor and becomes axial occupying the circular disc with external diameter equal to outer casing diameter and internal diameter equal to outer liner diameter (for the preliminary design);

- **Scaling procedure override.** If we impose the equality of non-dimensional flow rate with NASA combustor [28], the resulting scale factor is 2.162, however, applying it to the combustor dimensions yields a different *geometry configuration* than the combustor for the 100 kW MGT (Figure 6.6); that's because now the geometric constrains given by turbine engineers imply that the combustor outlet diameter must be 610 mm which is larger than the resulting inner liner/casing diameters.

  A quick calculation indicates that if the combustor mean diameter is set at 610 mm and 18 injectors are used[11], the pitch results 106 mm which is close to the pitch recommendation of GE design practices between 2.5 and 3.3 inches, i.e. between 63.5 and 0.084 mm. The mean diameter is kept at 610 mm and the outer and inner case diameters are calculated in order to obtain the same reference are of NASA combustor ($0.374m^2$), resulting respectively: $795mm$ and $394mm$. The outer and inner liner diameters are calculated to give the same case/liner proportions as for the 100 kW MGT combustor case; the resulting liner height is 129 mm. The liner height to injector pitch ratio results 1.216

[11]The choice for an even number of injectors aims to allow in the future an injection density study on performance and emissions, similar to that done by NASA [28].

which is close to unity and therefore in accordance with the recommendation of UNIGE team. To satisfy all these diameters, the design solution taken was to taper the inner liner and casing (Figure B).

We choose to maintain the reference area (i.e. the annular area between outer and inner casing) resulting from the equality imposition of the non-dimensional flow rates and adapt the combustor geometry aiming at attaining the GE Desing Practices, putting aside the scaling procedure for all dimensions except for the combustor outlet.

- This so-called *tapered geometry*, due to proximity with turbine casing, would cause part of the heat produced in the combustion chamber to *re-heat* the gases expanding in the turbine. That would increase the power output of the turbine but would cause thermal efficiency to drop if no recuperator is foreseen, as the case for the 1500 kW MGT[12]. In this case, we need to avoid turbine re-heating since it operates under the non-recuperated Brayton-Joule cycle. This calls for eliminating any recirculating or stagnation zones in the annulus, in proximity of the inner case tapered side.

- As explained, the inner liner had to be tapered to allow a combustion chamber with moderate mean diameter, the resulting inner curve connecting to the turbine is reduced to a rather short curve which apparently eliminates the need for cooling. Actually, the exiting flow would tend to recirculate and therefore create a stagnation zone in the combustion chamber in proximity of the inner curve that would both compromise the pattern factor and create a hot spot in the liner, for this reason, a row of dilution holes (which are always intended to generate cross flow jets) will be place in the inner curve to eliminate any recirculation zone and aid to uniform the flow. For preliminary design purposes, the corresponding cooling mass flow of inner curve is therefore accounted in the dilution air.

- According to GE Design Practices, the *straight liner length* is 2.5 times the liner height resulting 320 mm;

- Straight liner length to injector's pitch ratio results 3.0 which is larger than 2.5 and therefore in accordance with GE Design Practices;

- We adopt the combustor outlet width with 39 mm, resulting from the scaling procedure (k=2.162); the estimated combustor outlet velocity (v_{s3}) results

[12]For recuperated micro gas turbines combustors the tapered geometry could be used as an advantage for increased power production.

Table 6.14: Preliminary mass flow rates through liner combustor for 1500 kW MGT

Air function	% of total	Mass flow rate [kg/s]
Combustion (swirlers)	63.5	4.75
per swirler (18)	3.53	0.26
Dilution	24.3	1.44
Liner cooling	7.5	0.56
Dome cooling	1.8	0.14
Outer curve cooling	2.9	0.59
Inner curve cooling	-	-
Total	100	7.48

approximately 61 m/s which is acceptable since it is close to the estimated combustor outlet velocity for the 100 kW MGT (66 m/s);

- It is noted that the combustion air fraction increases from 32% to 64%, that's because the temperature rise the combustor needs to promote now (696 K) is roughly the double than in 100 kW model (330 K). As a consequence, less air remains to be divided for dilution and cooling purposes. That is not a real concern since the cooling air now is cooler than in the 100 kW MGT combustor. It is to be verified if dilution air (now 17.6% of total) will be enough to ensure a LOW pattern factor at outlet. Lefebvre indicates that dilution air is usually between 20 and 40% of total combustor airflow [24]; after accounting for the cooling mass flow of inner curve in the dilution air, the later results 24.3% which is above the minimum 20% of total combustor airflow recommended;
- Flow passages. The preliminary air division for the 1500 kW combustor are indicated in Table 6.14:
- Arbitrary openings are provided for fitting the 18 swirlers through which all the combustion air shall pass;
- Dilution rows. Since the liner is tapered the maximum dilution jet penetration required varies from row to row; it is predicted the use of two pairs of rows in the liner region where it is tapered, two rows in the straight outer liner and two rows in the the tapered inner liner; a fifth row is foreseen in the inner curve to eliminate any recirculation flow in the combustion chamber and help to reduce the pattern factor.
- Liner cooling. The distance between the slots is 80 mm which is in the interval recommended by the GE Design Practices (40 - 80 mm); Hole diameter of

liner cooling flows is set 5 mm which results in 36 holes per slots; there are still four(4) slots in the liner cooling;

- Outer curve cooling. Hole diameter is set 5 mm, the quantity is 144 evenly located in a single slot;
- Inner curve cooling. It is absent. The inner curve contains a row of dilution holes;
- Note that dilution and cooling holes quantities are multiples of the number of injectors (18).

Estimated velocities in different combustion chamber sections Recall from Section 6.7 that for designing the flow passages in the 100 kW MGT combustor the combustion chamber had to be divided in three sections, namely: 1) End of combustion zone; 2) Beginning of dilution zone and 3) Combustor outlet. The velocities in these sections resulted respectively: $6.83 m/s$, $7.846 m/s$ and $65.7 m/s$. In addition the velocity of exhaust gases leaving *dilution zone* as reported resulted $11.4 m/s$. Clearly, the flow accelerates because: the passage width reduces, the flow goes from a large radius to a smaller radius both diminishing the area and the specific mass reduces as the combustion takes place and the mixture temperature increases.

Turning our attention to the liner of the 1500 kW MGT combustor we note that it is tapered, i.e. the liner height in correspondence of the dilution jets varies, as the maximum jet penetration. In addition, recall from Section 6.8 that the procedure to determine the number and the diameter of the dilution holes involved: a) for the number of holes the use of the mean velocity inside the liner in the section where the dilution jets penetrate and b) for the corresponding hole diameters, the mass flow rate and mean velocity in the annulus right before the air enter the dilution holes, among other things; all these parameters change at each dilution row section. For these reasons, it was necessary to divide the combustion chamber in a certain number of sections and estimate the flow velocities and properties in each (including temperature and specific mass that changes due to mixture with film cooling streams and combustion); the estimation of flow velocities in the annulus was also possible since we have predetermined not only the annulus geometry (based on the previous section) but also the preliminary air division for the (four) liner cooling slots and each (of the five) dilution rows. The combustion chamber for the 1500 kW MGT was divided in five sections (see Figure in Appendix B): 1) End of combustion zone; 2.1) Beginning of dilution zone (coincident with first dilution row); 2.2) Second dilution row section; 2.3) Beginning of combustion chamber curve and 3) Combustor outlet (the throat, since it is the minimum flow passage area).

After having calculated the aforementioned data shown, we arbitrarily stipulated a maximum jet penetration of 55% in stations (2.1) and (2.2) whose local liner heights are respectively 110 mm and 52 mm, resulting in eighteen (18) holes per each dilution row (there are four, two in each station). One may argue that this is a small value, however it results from the procedure explained in previous section mainly as a consequence of the small dilution flow rate (24.3% of total air flow rate). Increasing jet penetration above %55 would reduce further the amount of holes and thus it is recognized that the estimated %55 penetration with 18 dilution holes per row is a good starting point for the premilinary design before the first CFD calculations are used to indicate more correct values that yield good mixing and the predicted amount of air used. With regard to the dilution holes diameter, it results 12 mm.

The determination of the dilution holes quantity and diameter cited above excluded one fifth of air that is to be dedicated to the remaining dilution row responsible for final mixing and eradication of any recirculation zone close to combustor outlet (as mentioned in item 6.10). Such remaining air stream is not subjected to the flow conditions necessary for the procedure outlined in Section 6.8 to apply. In this case is was supposed that the same amount of dilution holes per row with the same diameter would suffice for defining a preliminary design (see Appendix B). The successive CFD calculations might indicate more correct values that eliminate recirculation zones and reduces the pattern factor to a minimum while using the the predicted amount of air, i.e. one-fifth of dilution that corresponds to $0.364 kg/s$.

The outer curve and liner cooling flow passages with combustion chamber location, quantity of holes[13] and diameters are indicate in the Figure of Appendix B.

6.11 Quoted drawings

The quoted drawings of the reverse flow annular combustor for the 100 kW and 1500 kW micro gas turbines in their preliminary design *status* are shown in Figures 6.6 and Appendix B.

[13] Calculated as for the 100 kw MGT combustor, using an roughly estimated discharge coefficient of 0.7.

6.12 Summary

The micro gas turbine operates in the Brayton-Joule cycle (Figure 6.1) and the combustion inside the combustion chamber is assumed, for simplicity on the preliminary design phase, to follow the global reaction:

$$\mathrm{CH_4} + (\tfrac{\chi_{\mathrm{CO_2}}}{\chi_{\mathrm{CH_4}}})\mathrm{CO_2} + (\tfrac{\chi_{\mathrm{N_2}}}{\chi_{\mathrm{CH_4}}})\mathrm{N_2} + \tfrac{2}{\Phi}(\mathrm{O_2} + 3{\cdot}76\,\mathrm{N_2}) \longrightarrow$$
$$(1 + \tfrac{\chi_{\mathrm{CO_2}}}{\chi_{\mathrm{CH_4}}})\mathrm{CO_2} + 2\,\mathrm{H_2O} + 2\,(\tfrac{1\text{-}\Phi}{\Phi})\mathrm{O_2} + (\tfrac{7{\cdot}52}{\Phi} + \tfrac{\chi_{\mathrm{N_2}}}{\chi_{\mathrm{CH_4}}})\mathrm{N_2}.$$

First of all, the preliminary design of a reverse flow combustor for a micro gas turbine consists in the **collection of relevant data**:

1. The boundary conditions given by the compressor and turbine engineering team which are indicated in Table 6.1;

2. The geometrical constrains that the combustor shall respect given by the compressor and turbine engineering team, indicated in Figure 6.2;

3. The fuels that the combustor may utilize, indicated in Table 6.3;

4. A combustor design on which to base ours; we note that the base design of Ref.: [28], to which we refer as NASA combustor, uses simplex pressure-atomizing injectors of kerosene Jet-A, and since it requires additional times for atomization, evaporation and mixing it has longer combustion zones than our design would actually require, such that basing our design on theirs would yield conservative results, i.e. longer combustion zones that actually necessary; in addition their boundary conditions (Table 6.4) and main dimensions (Figure 6.3) are also data useful in the subsequent scaling procedure;

5. Thermodynamic data regarding the fuel and combustion itself, whose determination follows the steps:

   a) The specific heat of dry air with known composition at combustor inlet temperature '$c_{p,a}$' is initially determined;

   b) Based on the composition, the lower heating value of the fuel could be determined;

   c) Fuel composition and a set injection pressure slightly above the combustor inlet pressure allowed the determination of fuel injection conditions such as: injection temperature and fuel specific mass;

d) The fuel-to-combustor air ratio f is determined afterwards using an energy balance in the combustion chamber;

e) Given the desirability of operating with Lean Pre-mixed flame in the combustion zone, an equivalence ratio of 0.5 was chosen. Together with the stoichiometric Air-to-Fuel ratio (known after the definition of global reaction) it was possible to determine the Air-to-Fuel Ratio (AFR) in the combustion zone. The combustion air fraction α, i.e. the fraction of total air estimated to participate in the combustion was then calculated based on knowledge about fuel-to-combustor air ratio f.

6. After the combustion air fraction has been calculated, the remaining dilution and cooling air fractions $(1 - \alpha)$ is arbitrarily split among the other passages such as outer curve, inner curve etc., according to the contribution each passage had relative to the sum of all other fractions in the NASA design (Table 6.6). We assumed that this fractions will be able to promote dilution and cooling satisfactorily in a preliminary approach, but in the design optimization phase these fractions might be updated, Chapter 7 shows how the preliminary design is modified such that these fractions are obtained. The preliminary air partitioning is summarized in Table 6.10 and indicated in Figure 6.4.

Afterwards the **dimensioning phase** takes place. For the 100 kW MGT combustor this phase is summarized below:

1. By imposing the equality of *non-dimesional mass flow* ($\dot{m}\sqrt{T_0}/A_{ref}P_0$) of NASA combustor and ours, instead of using the *load parameter* whose scaling approach was shown to be inappropriate in this case, we could obtain the scaling factor (0.913) between the combustors. With this approach we expect the total pressure loss of both combustors to be equal or very similar (1.7%). The scaled main dimensions were summarized in Table 6.12. We override some scaled dimensions in order to satisfy the following design practices recommended by experts:

   a) The straight liner lenght 'L_c' to liner height 'H_l' ratio is set equal to 2.5;

   b) the lenght of combustion zone is set equal to 'H_l';

2. Afterwards, various air passages to the combustion chamber are designed according to the guidelines:

   a) Assume a total pressure drop across the liner which may apply preliminary to design all passages, as mentioned earlier, we have assumed 1.7% of inlet total pressure;

b) Individuate three control sections inside the combustion chamber: (1) end of combustion zone (before dilution and mixing with cooling films of liner and dome occur); (2) beginning of dilution zone (where the products from section (1) have mixed with cooling film of liner and dome, but are not yet diluted) and (3) combustor outlet;

c) For each section of item 2b determine temperature, specific mass, mass flow rate and specific heat; for sections (2) and (3) also determine the average molecular weight and gas constant; determine also the mole flow rate in section (3); these parameters may be used subsequently; they could be calculated based on the preliminary air partitioning (Table 6.11) and the knowledge about composition of air, fuel, and products (see global reaction in the beginning of the Chapter) streams, where complete combustion has been assumed;

d) Estimate the velocity inside the liner at the entry of dilution zone — Section (2) — by using continuity equation with the specific mass and mass flow rate calculated in this section and the liner area (obtained after item 1);

e) The dilution holes are split, for the current design, in 2 rows at the outer liner and 2 rows at the inner liner, counter-opposed for enhanced mixing; initially it is stipulated a 72% penetration of the dilution jets (measured as percentage of liner height); after having calculated the effective jet diameter by using a correlation it's possible to determine the total number of dilution holes based on the Cranfield Method; we use a second correlation that allows the calculation of the discharge coefficient based on the ratio of hole mass flow rate to annulus mass flow rate and the ratio of the jet dynamic pressure to the annulus dynamic pressure upstream of the holes; such approach applies to the discharge coefficient for the inner and outer liners; a third correlation is used to determine the actual hole diameters; data gathered in item 2c is used in this stage.

f) The preliminary design assumes that cooling air indicated in Table 6.11 is enough to avoid hotspots in the dome, liner and curve sections; the dimensioning procedure can be divided in two:

   i. The diameter and number of holes for cooling the liner and the inner and outer curve sections comes after we assume a discharge coefficient (0.7), equal for all of these passages (splash-cooling ring), and choose the diameter of holes (2 mm) such that the quantity of holes resulted meet not only the effective flow area requirement but the multiplicity

requirement for facilitating the numerical simulation of the combustor flow field using the periodic boundary condition;

Meaningful data related to the preliminary design of the combustors for the 100 kW and 1500 kW micro gas turbines are summarized in Table 6.15 while the quoted drawings of the prelimary designs are shown in Figure 6.6 and Appendix B.

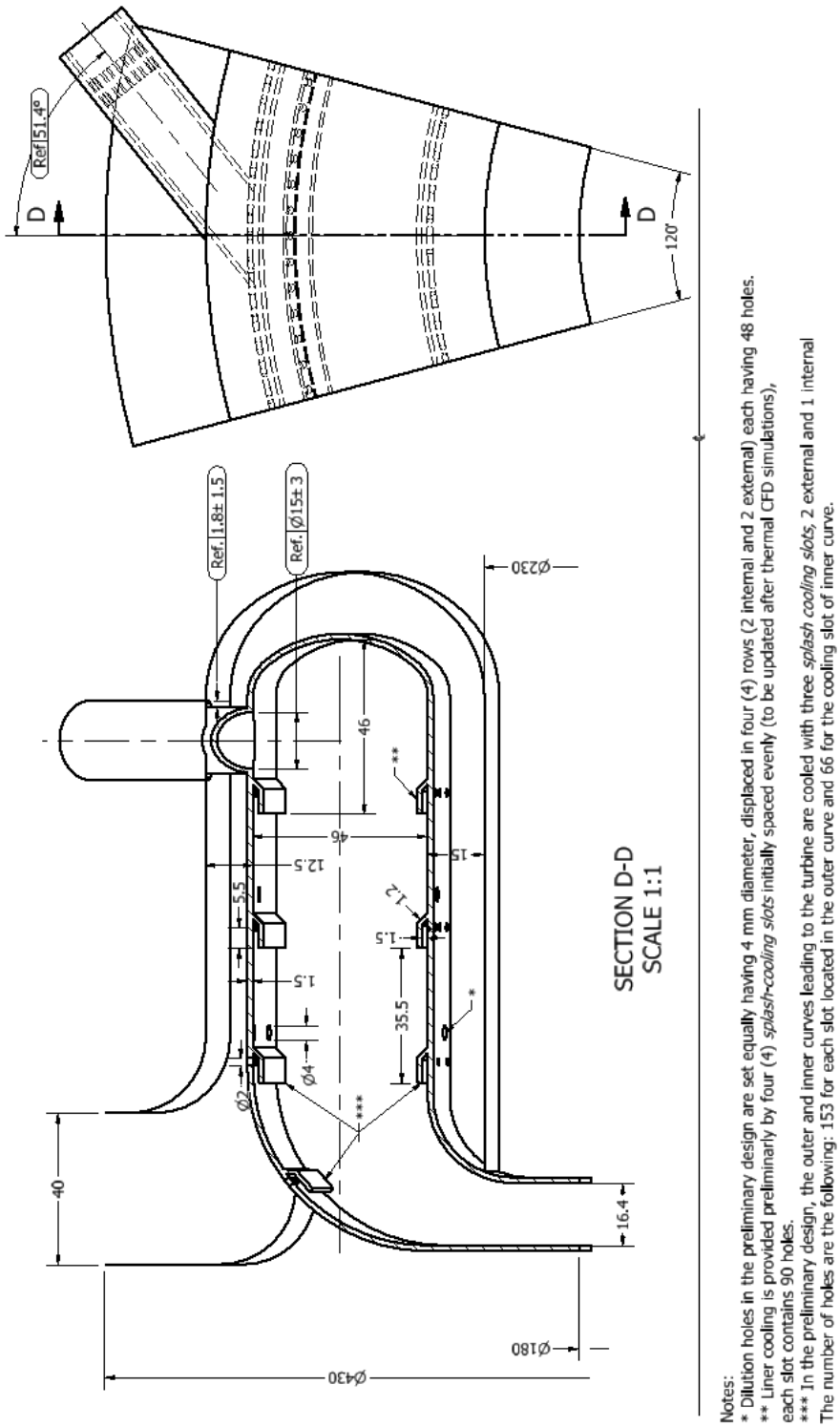

Figure 6.6: Quoted drawing of the reverse flow annular combustor for the 100 kW MGT in its preliminary design status with reference values for the subsequent swirler design

Table 6.15: Meaningful data related to the preliminary design

Parameter	NASA [28]	$100kW$	$1500kW$	Unit
	Boundary conditions			
Mass flow rate of air at inlet	3.63	0.72	7.48	kg/s
Inlet total pressure (P_{05})	1620	430	612	kPa
Outlet static pressure (P_3)	-	420.1	599.2	kPa
Inlet total temperature (T_{05})	717	893.15	527.00	K
Outlet total temperature (T_{03})	1176.47 [14]	1223.15		K
	Design point data			
(DeltaPt/Pt_in)		1.7 [15]		%
Fuel	Jet-A (L)	Natural Gas		
Combustion efficiency		100		%
Primary air fraction	0.3608	0.3228	0.6353	
Fuel/air ratio	0.0140	0.0096	0.0189	
Equivalence ratio in primary zone	0.52	0.50		
	Scaling approach			
Non-dimensional flow rate		7.50E-04		
Resulting scale factor		0.913 [16]	Override [17]	
	Main dimensions			
Outer casing diameter	0.406	0.371	0.795	m

[14]Temperature at combustor outlet has been calculated from an energy balance using the typical average specific heat of combustion gases $C_p = 1.148kJ/kg.K$ (Ref.: [36]), since it would not interfere with the preliminary design, and the low heating value of kerosene Jet-A $LHV = 18400BTU/lb$ (Ref.: [38]).

[15]Recall, total pressure drop is expected to be equal to that of NASA combustor since we have imposed the equality of non-dimensional flow rate and all three combustors share the same typology: reverse-flow annular.

[16]The scale factor based on the equality of load parameters (8.19×10^8) results 0.907 which is similar to 0.913, the scale factor originated from the non-dimensional flow rate equality.

[17]As explained in Section 6.10, the 1500 kW combustor could not be directly scaled from NASA combustor.

Parameter	NASA [28]	$100kW$	$1500kW$	Unit
Outer liner diameter	0.385	0.352	0.739	m
Inner liner diameter	0.285	0.260	0.480	m
Inner casing diameter	0.252	0.230	0.394	m
Combustor mean diameter	0.335	0.306	0.610	m
Combustor inlet diameter		0.430	-	m
Combustor inlet width	Not applicable	0.1100	-	m
Combustor outlet diameter		0.180	0.610	m
Combustor outlet width	0.018	0.0164	0.0389	m
Liner overall length	0.215	0.162	0.384	m
Liner straight section lenght 'Lc'	Not available	0.114	0.324	m
Liner height 'H_l'	0.050	0.046	0.129	m
Injectors pitch 'b'	0.058		0.106	m
H_l/b	0.86	Not applicable	1.216	
Lc/b	Not available		3.04	
Lc/H_l		2.5		
Primary zone axial length $L_{primary}$ to H_l ratio	Not available	1	1	
Number of injectors	18	3 [18]	18 [19]	
Preliminary design values				
Dilution flow				
Penetration of dillution jets with respect to channel height	Not available	72.0	55.0	%
Number of holes		192	90 [20]	
Hole diameter		4	12	mm

[18] Distributed tangentially with respect to the liner.
[19] Distributed axially with respect to the liner.
[20] Eighteen (18) holes per each of the five dilution rows.

Parameter	NASA [28]	$100kW$	$1500kW$	Unit
Liner Cooling flow				
Number of holes in each of the four slots	Not available	90	198	
Hole diameter			2	mm
Inner and outer turn sections (curves) cooling flows				
Number of holes in each ot the two slots in the outer curve	Not available	153	342	
Number of holes in the inner curve slot		66	-	
Hole diameter			2	mm
Results expected after numerical simulations				
Reference values				
Reference velocity	5.79	6.47	4.97	m/s
Reference dynamic pressure	131.5	34.9	49.67	Pa
Mass flow rates				
Mass flow rate of fuel	0.051	0.007	0.141	kg/s
Mass flow rate of air dedicated to Combustion (combustion zone)	1.310	0.232	4.75	kg/s
Mass flow rate of air dedicated to Dilution	1.118	0.236	1.82	kg/s
Mass flow rate of air dedicated to Cooling	1.203	0.254	0.91	kg/s
Mean velocities				

Parameter	NASA [28]	$100kW$	$1500kW$	Unit
Velocity in the liner assuming reactants flow	11.0 [21]	3.3		m/s
Velocity in the liner assuming products flow	26.2 [22]	7.0	See appx B.	m/s
Velocity in the outer annulus after entering CC	Not applicable	26.8		m/s
Velocity of exhaust gases leaving dilution zone	Not available	11.40		m/s
Velocity of exhaust gases leaving the combustor	79.6 [23]	65.7		m/s

[21] We estimate the density of gases leaving the primary zone equal to our calculated cases. The resulting value is an average between 6.46 m/s and 15.45 m/s.

[22] We estimate the density of gases leaving the primary zone equal to our calculated cases. The resulting value is an average between 19.5 m/s and 33.0 m/s.

[23] The specific mass required for the estimation of such velocity comes from an assumption of typical exhaust gas constant $R = 0.287kJ/kg.K$ and a rough approximation of NASA combustor outlet area based on Figure 6.3.

Chapter 7

Design Refinement

We'll use a Computational Fluid Dynamics commercial software to improve the preliminary design of the combustor in two phases, using increasing level of simulation complexity. The equations solved at this stage were shown in Section 4.1.

1. Steady flow non-reactive multi-species simulations;
2. Steady reactive flow simulations;
3. Steady reactive flow with conjugate heat transfer through walls simulations.

Initially, we'll show how the preliminary design is modified such that the flow rate fractions directed for cooling, dilution and primary air (combustion) are obtained after a series of non-reactive CFD simulations are carried out. The preliminary air partitioning is summarized in Table 6.10.

Secondly, we'll refine the design of the injector design adopted up to the design 19 (the last indicated in Table 7.1) with the strategies shown at the end of Section 4.6 for allowing either biogas or natural gas utilization.

Only when the flame has been observed to be stable due to a refinement in the injector's design that we can actually move our attention to hotspots elimination and reduction of pattern factor, this stage would involve repositioning and diameter modification of cooling and dilution passages. Other improvements on the combustion chamber such as liner thickness modification and internal/external diameters could also be put in practice as soon as the injector is optimized in order to, let's say reduce stress in the liner and reduce overall pressure losses.

7.1 Models applied in the CFD simulations

The proper numerical technique to be employed for a numerical solution depends on the mathematical behavior of the governing equations. We note that the complete Navier-Stokes equations shown in Chapter 4 — Eqs. (4.9), (4.19) and (4.21) — have mixed hyperbolic, parabolic and elliptic behavior[16]. The *pressure correction technique* is embodied in the SIMPLE (Semi-Implicit Method for Pressure Linked Equations) algorithm developed by Patankar and Spalding with wide applications for both compressible and incompressible flows, including viscous flows which are governed by the complete Navier-Stokes equations[16]; this algorithm will be used in our steady flow CFD simulations.

7.1.1 Turbulence models

We deal with turbulence by using the RANS (Reynolds Averaged Navier Stokes) equations and the realizable $k - \epsilon$ model.

Such model seems appropriate for modelling the flow inside the combustion chamber, since despite the main core tangential flow developed by the injectos as we shall see, there are present numerous secondary flows.

"Both the realizable and RNG $k-\epsilon$ models have shown substantial improvements over the standard $k - \epsilon$ model where the flow features include strong streamline curvature, vortices, and rotation. Since the model is still relatively new, it is not clear in exactly which instances the realizable $k - \epsilon$ model consistently outperforms the RNG model. However, initial studies have shown that the realizable model provides the best performance of all the $k - \epsilon$ model versions for several validations of separated flows and flows with complex secondary flow features.[21]"

In addition, flows in which the vorticity is subjected to turbulent fluctuations may benefit from the realizable $k - \epsilon$ model.[12]

Production limiters

As pointed in the literature, "a disadvantage of standard two-equation turbulence models is the excessive generation of the turbulence energy, in the vicinity of stagnation points. In order to avoid the buildup of turbulent kinetic energy in the stagnation regions, the production term in the turbulence equations can be limited [20]" by the use of production limiters. This option has been enabled in the CFD software.